Supporting Information

Radical-Radical Coupling Effects in the Direct-Growth Grafting-Through Synthesis of Bottlebrush Polymers using RAFT and ROMP

*Mohammed Alaboalirat [a,b] Clark Vu [a,b] and John B. Matson [a,b]**

[a]Department of Chemistry, Virginia Tech, Blacksburg, Virginia 24061, United States

[b]Macromolecules Innovation Institute, Virginia Tech, Blacksburg, Virginia 24061, United States

E-mail: jbmatson@vt.edu

Scheme S1. Synthesis of Norbornene-functionalized trithiocarbonate **3**[a]

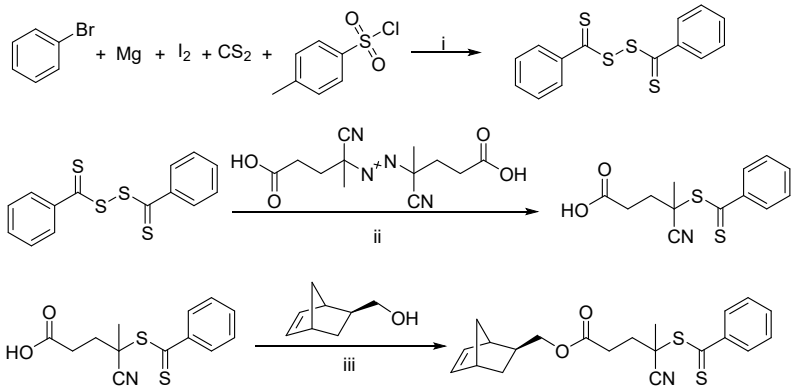

[a]Conditions: (i) THF, rt, 8 h. (ii) THF, 80 °C, 18 h. (iii) CH_2Cl_2, rt, 16 h.

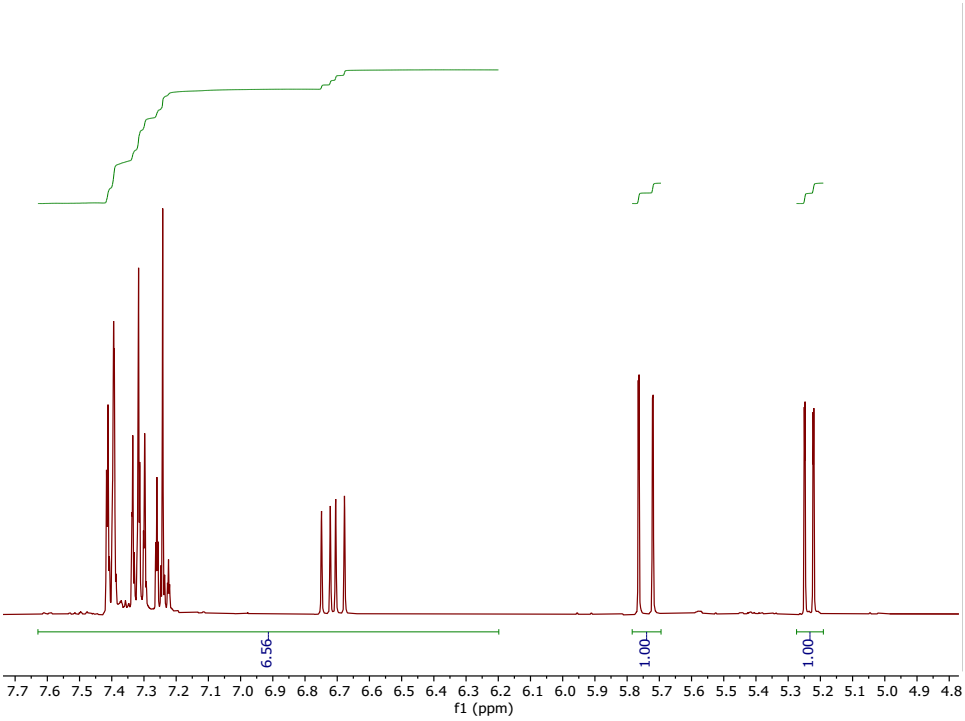

Figure S1. ^{1}H NMR spectrum showing crude aliquot of $\mathbf{S^{10\%}}$ containing unreacted monomer and MM after RAFT polymerization reaching a monomer conversion of 10%.

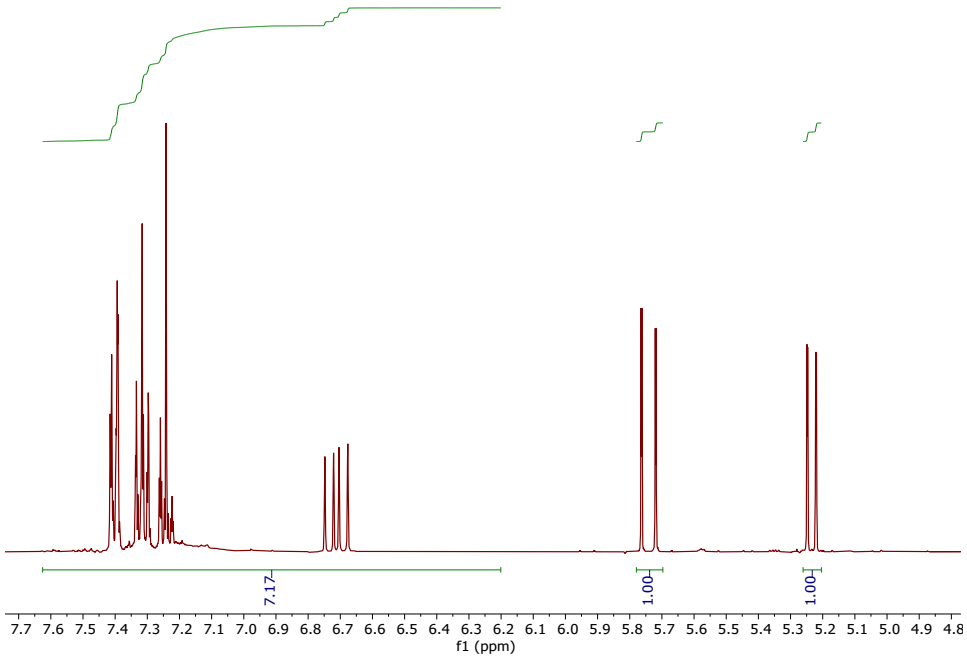

Figure S2. ^{1}H NMR spectrum showing crude aliquot of $\mathbf{S}^{20\%}$ containing unreacted monomer and MM after RAFT polymerization reaching a monomer conversion of 19%.

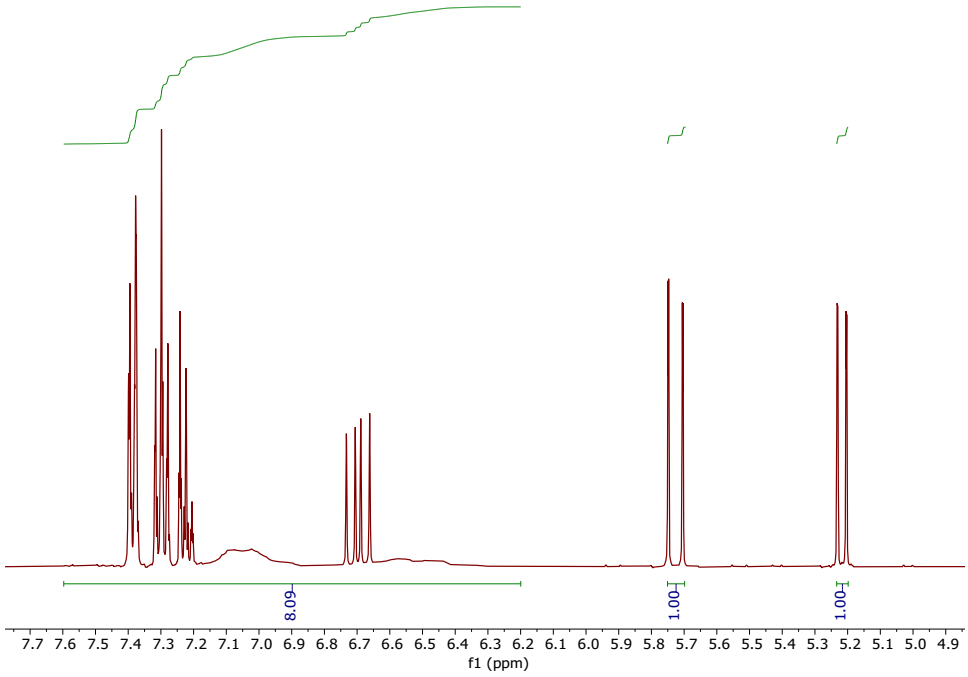

Figure S3. ^{1}H NMR spectrum showing crude aliquot of $\mathbf{S}^{30\%}$ containing unreacted monomer and MM after RAFT polymerization reaching a monomer conversion of 30%.

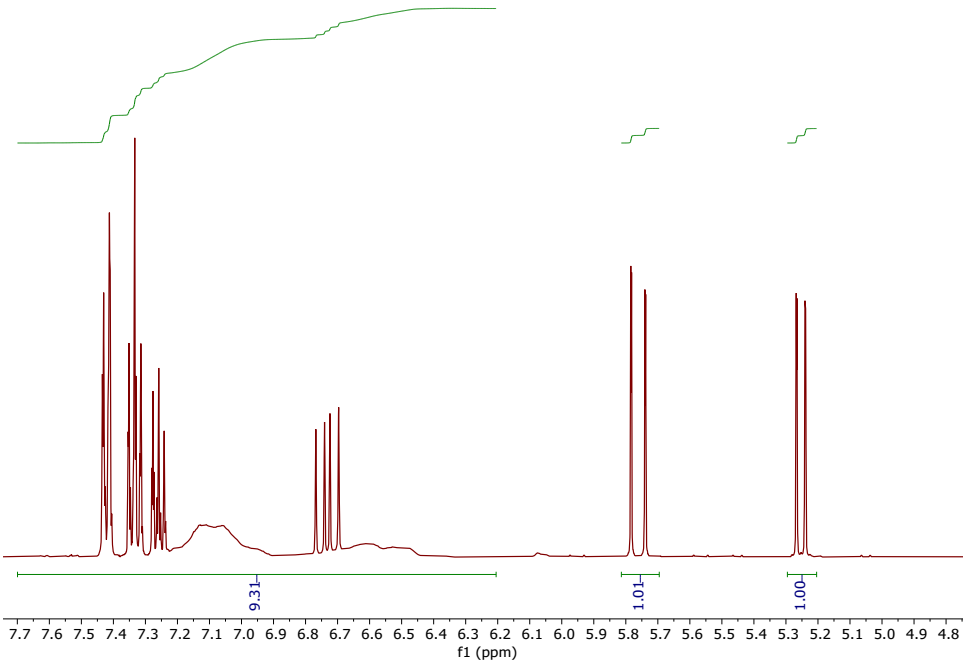

Figure S4. ^{1}H NMR spectrum showing crude aliquot of $\mathbf{S^{40\%}}$ containing unreacted monomer and MM after RAFT polymerization reaching a monomer conversion of 40%.

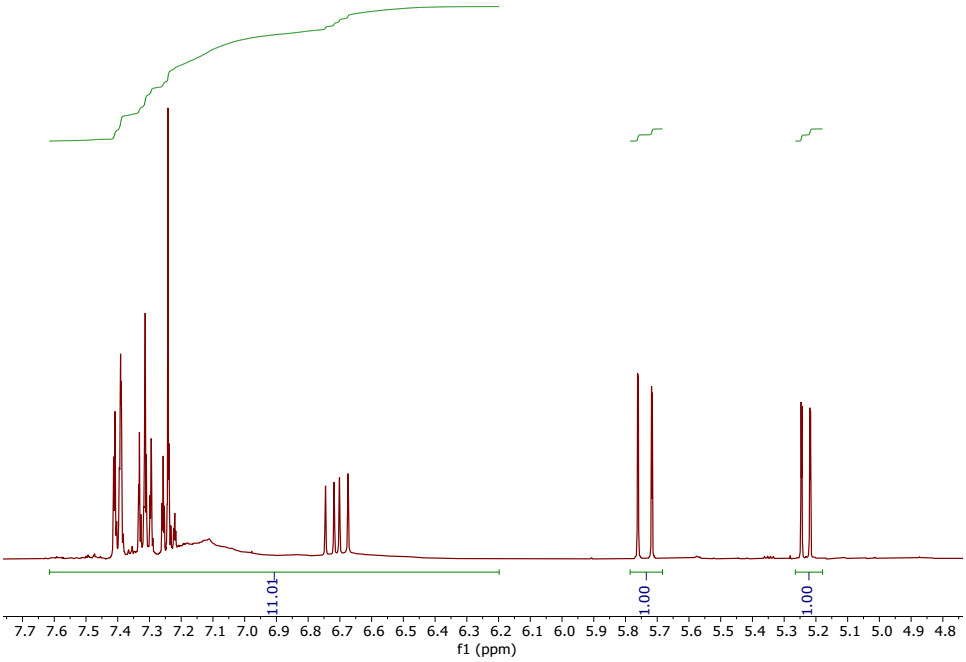

Figure S5. ^{1}H NMR spectrum showing crude aliquot of $\mathbf{S^{50\%}}$ containing unreacted monomer and MM after RAFT polymerization reaching a monomer conversion of 50%.

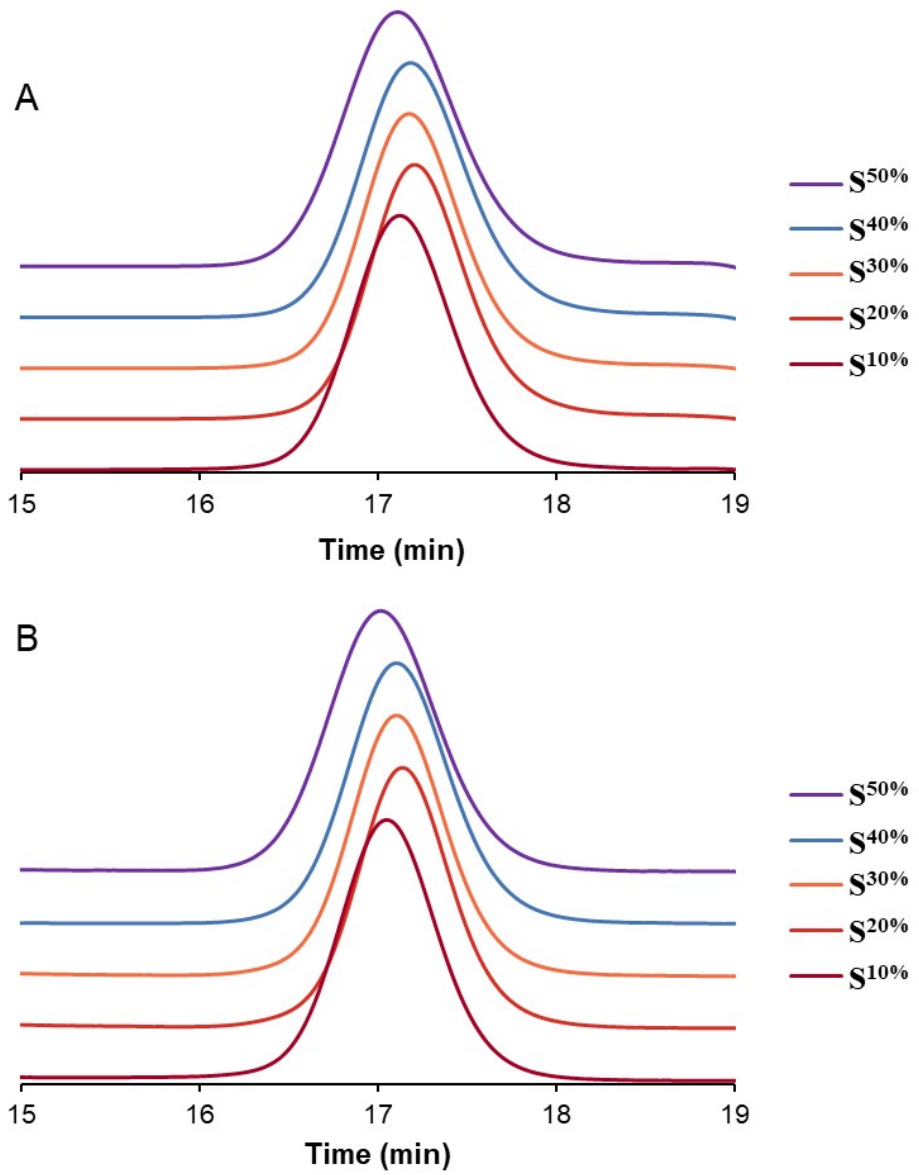

Figure S6. SEC traces showing (A) refractive index detector and (B) light scattering detector of PS MMs $\mathbf{S^{10\%}}$, $\mathbf{S^{20\%}}$, $\mathbf{S^{30\%}}$, $\mathbf{S^{40\%}}$ and $\mathbf{S^{50\%}}$.

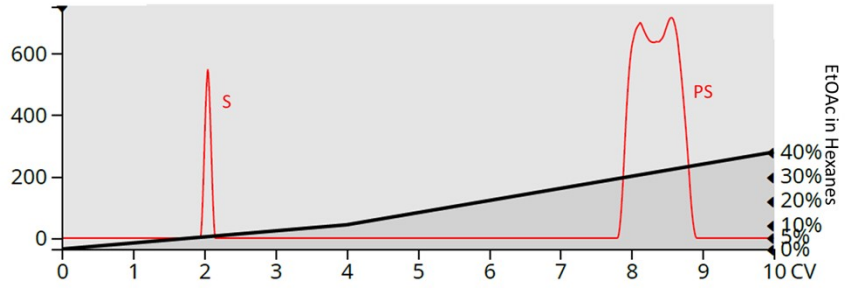

Figure S7. PS-MM purification plot showing the absorption of monomer and the MM at 200 nm (red) as the polarity of the mobile phase increases.

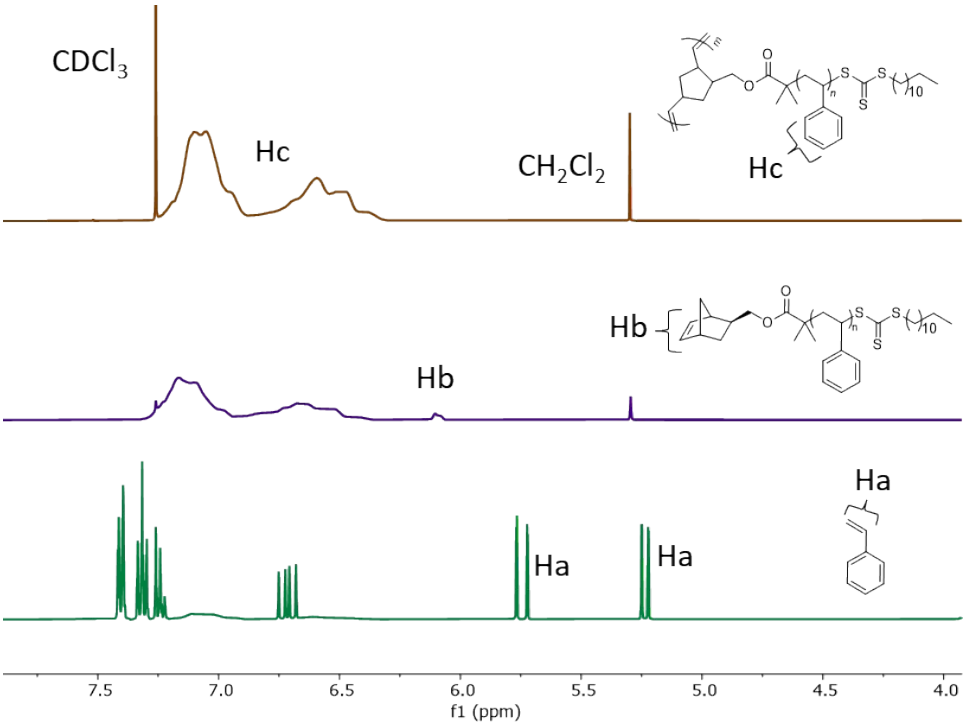

Figure S8. ^{1}H NMR stacked spectra showing the progress of $S_{100}^{30\%}$ from crude MM containing unreacted monomer after RAFT polymerization (bottom) to purified PS-MM after silica column (middle) and to PS-BB after ROMP (top).

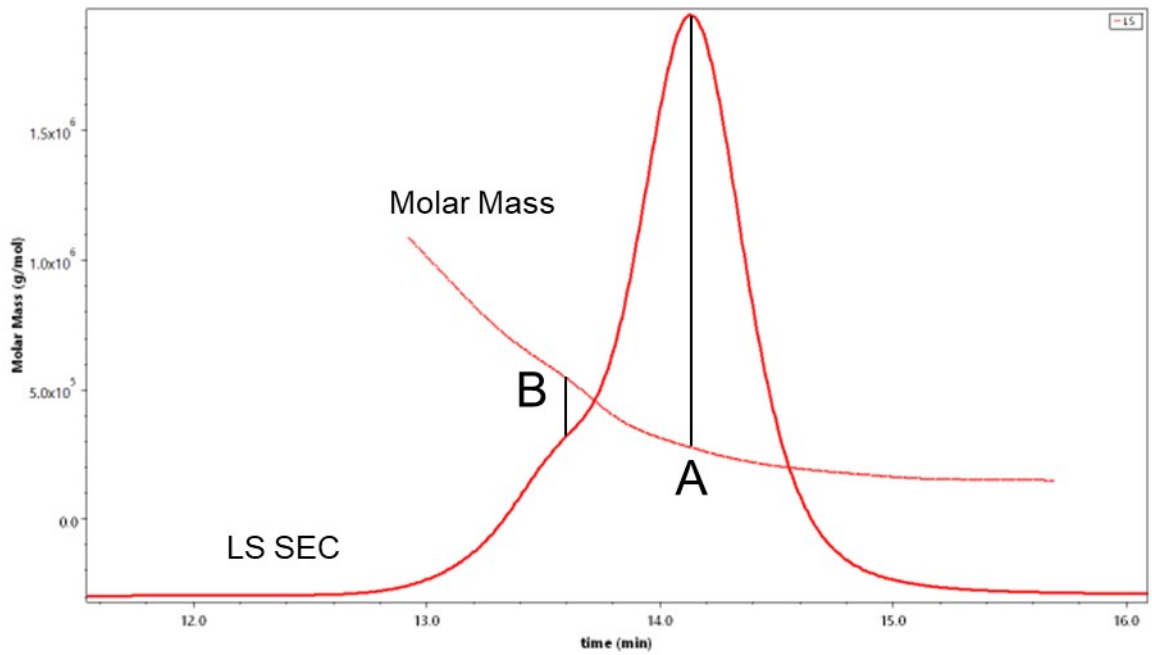

Figure S9. SEC trace of light scattering detector and molar mass of bottlebrush polymer $S_{100}^{20\%}$. The molar mass of peak A is 273 kg/mol and peak B is 518 kg/mol.

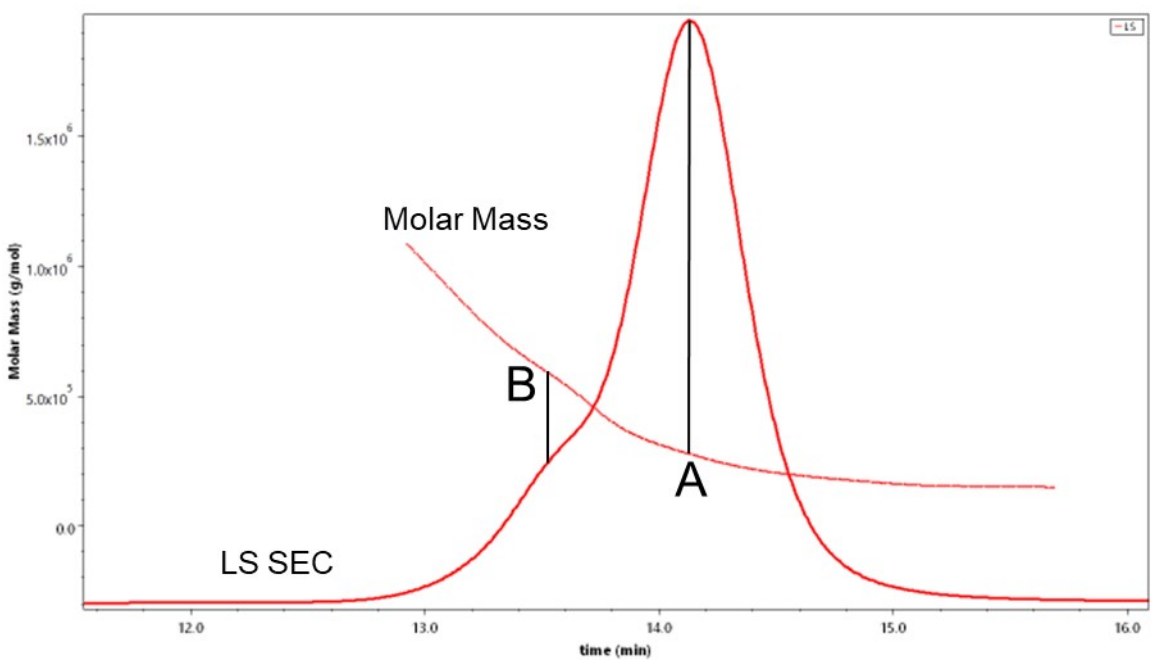

Figure S10. SEC trace of light scattering detector and molar mass of bottlebrush polymer $S_{100}^{30\%}$. The molar mass of peak A is 276 kg/mol and peak B is 572 kg/mol.

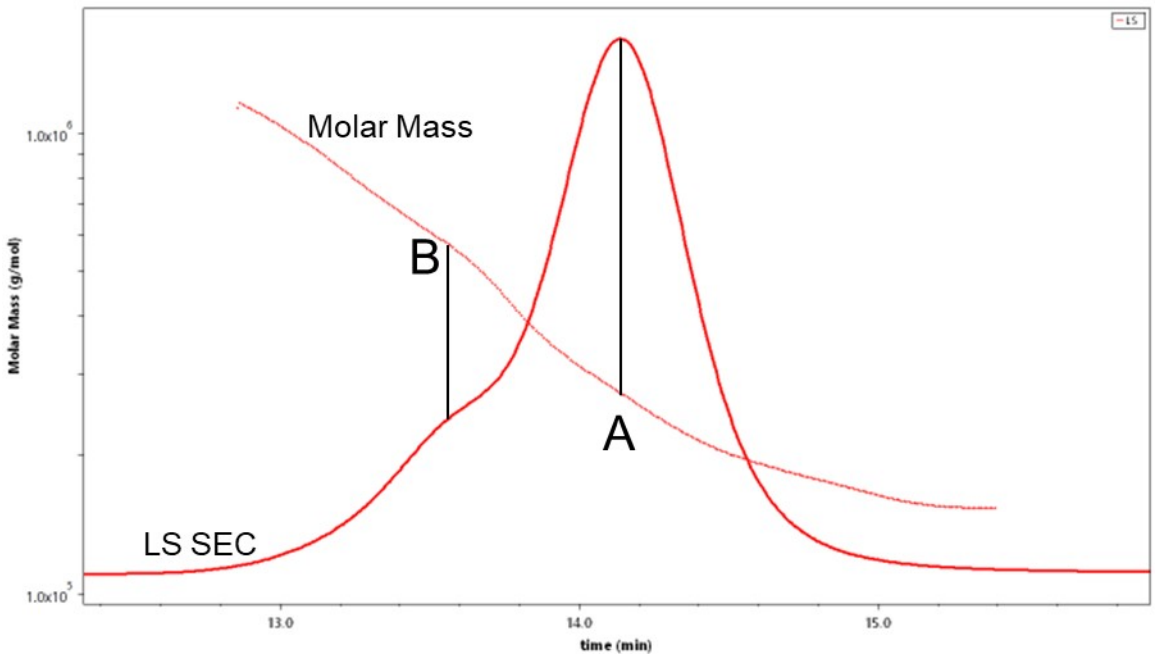

Figure S11. SEC trace of light scattering detector and molar mass of bottlebrush polymer $S_{100}^{40\%}$. The molar mass of peak A is 279 kg/mol and peak B is 574 kg/mol.

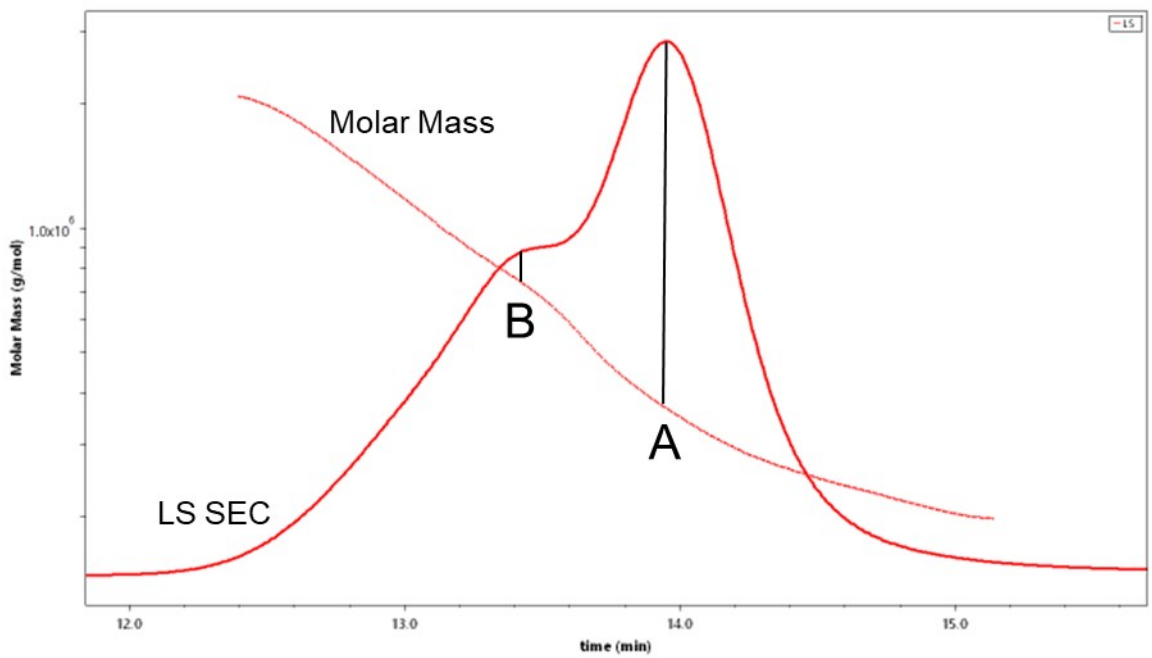

Figure S12. SEC trace of light scattering detector and molar mass of bottlebrush polymer $S_{100}^{50\%}$. The molar mass of peak A is 279 kg/mol and peak B is 524 kg/mol.

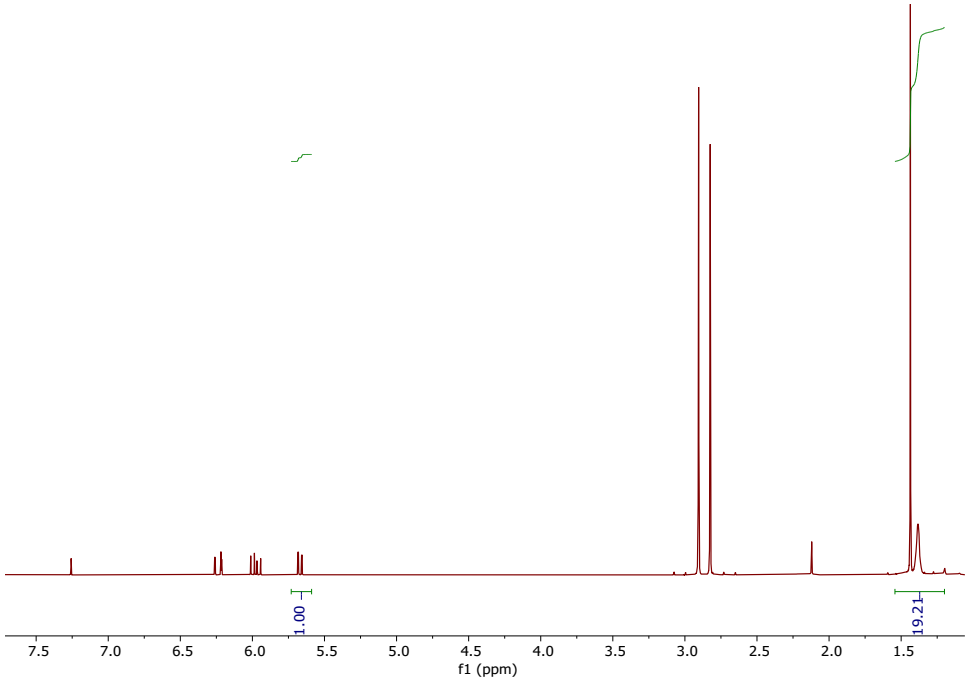

Figure S13. ^{1}H NMR spectrum showing crude aliquot of $\mathbf{T^{50\%}}$ containing unreacted monomer and MM after RAFT polymerization reaching a monomer conversion of 53%.

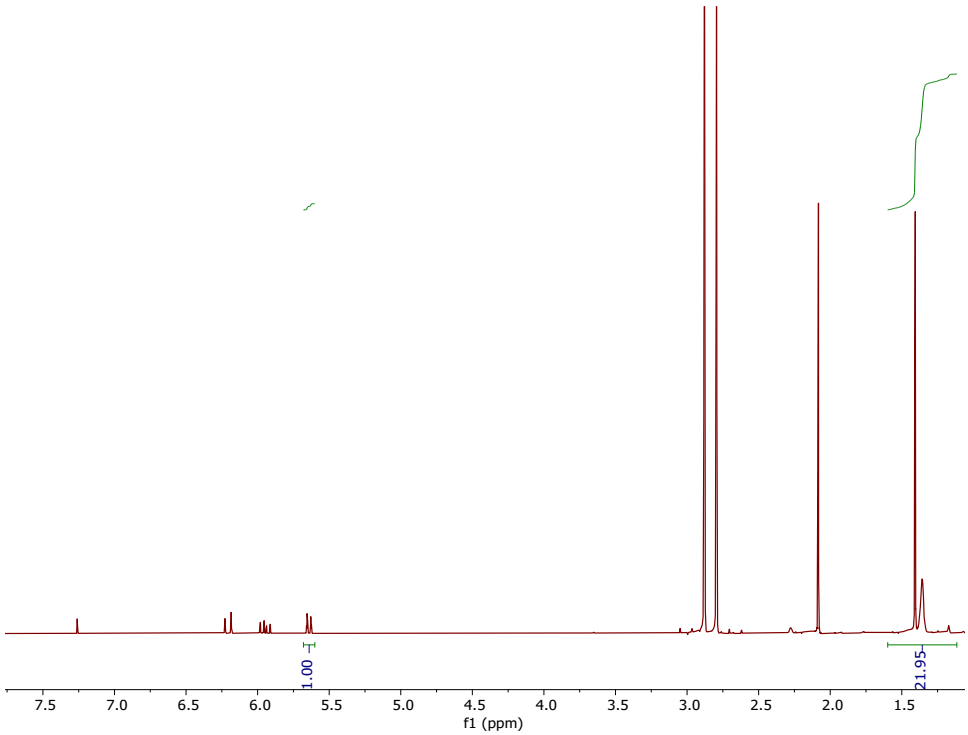

Figure S14. ^{1}H NMR spectrum showing crude aliquot of $\mathbf{T}^{60\%}$ containing unreacted monomer and MM after RAFT polymerization reaching a monomer conversion of 59%.

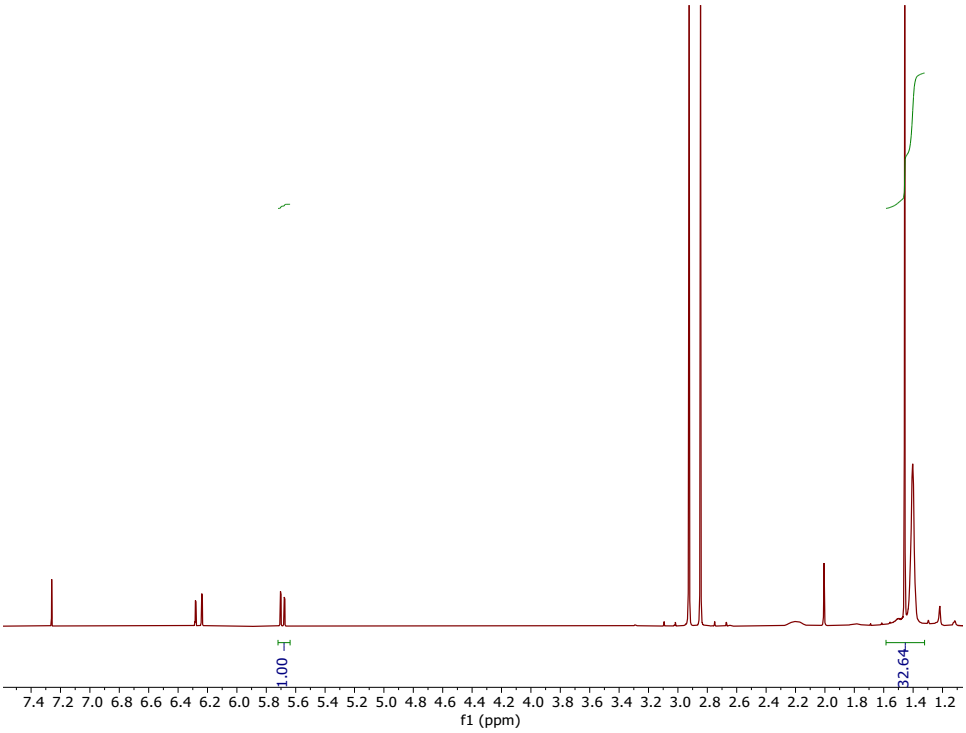

Figure S15. ^{1}H NMR spectrum showing crude aliquot of $\mathbf{T}^{70\%}$ containing unreacted monomer and MM after RAFT polymerization reaching a monomer conversion of 72%.

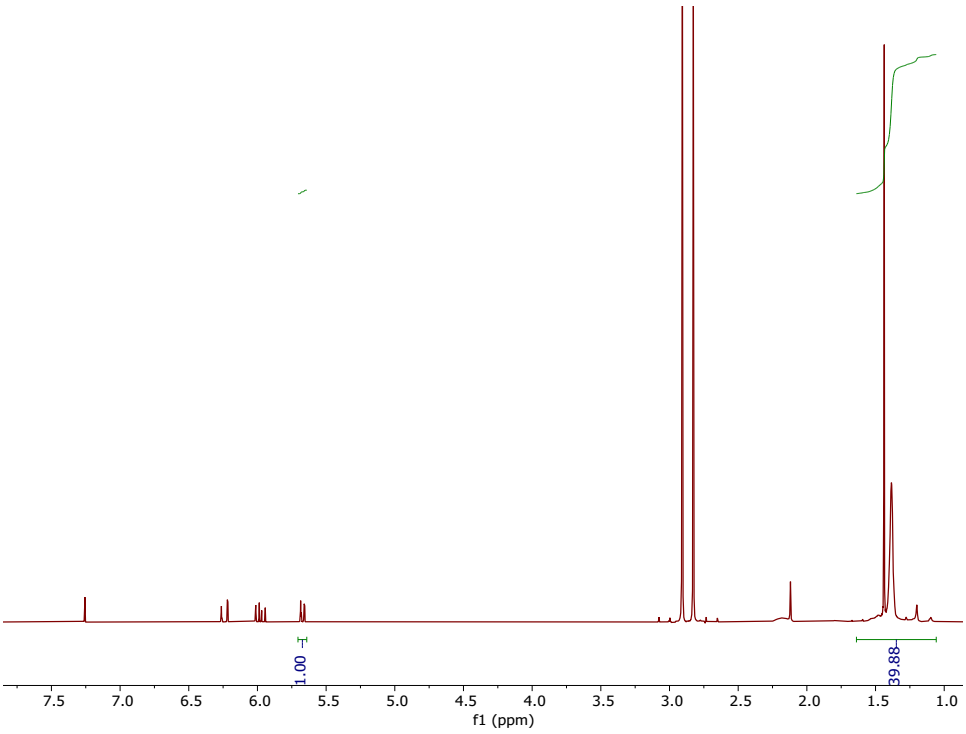

Figure S16. ^{1}H NMR spectrum showing crude aliquot of $\mathbf{T^{80\%}}$ containing unreacted monomer and MM after RAFT polymerization reaching a monomer conversion of 77%.

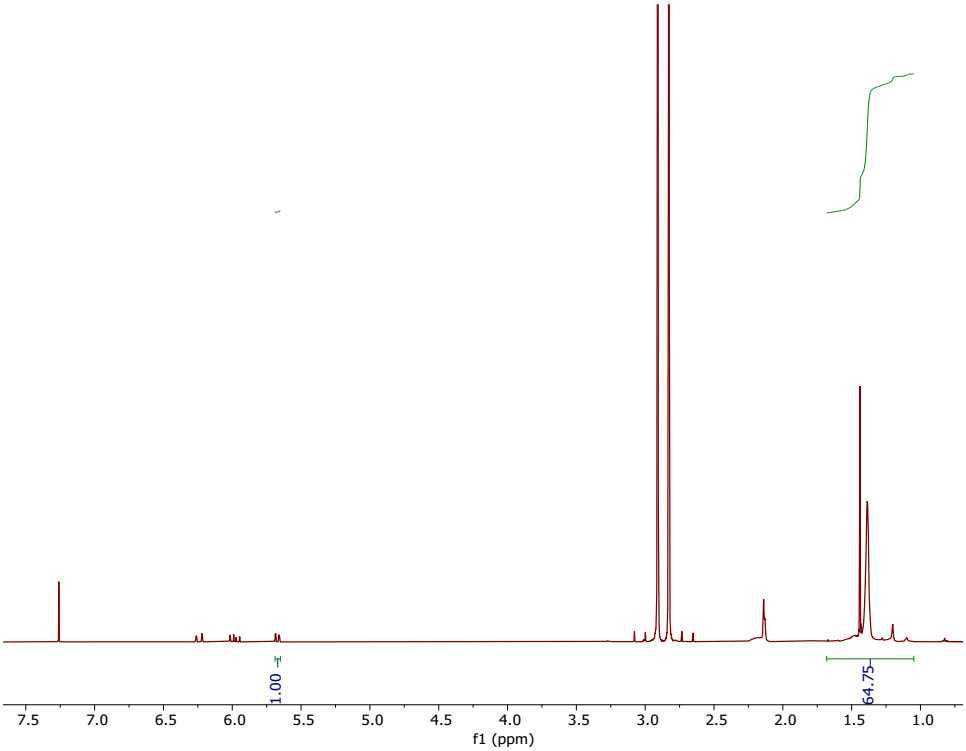

Figure S17. ^{1}H NMR spectrum showing crude aliquot of $\mathbf{T^{90\%}}$ containing unreacted monomer and MM after RAFT polymerization reaching a monomer conversion of 86%.

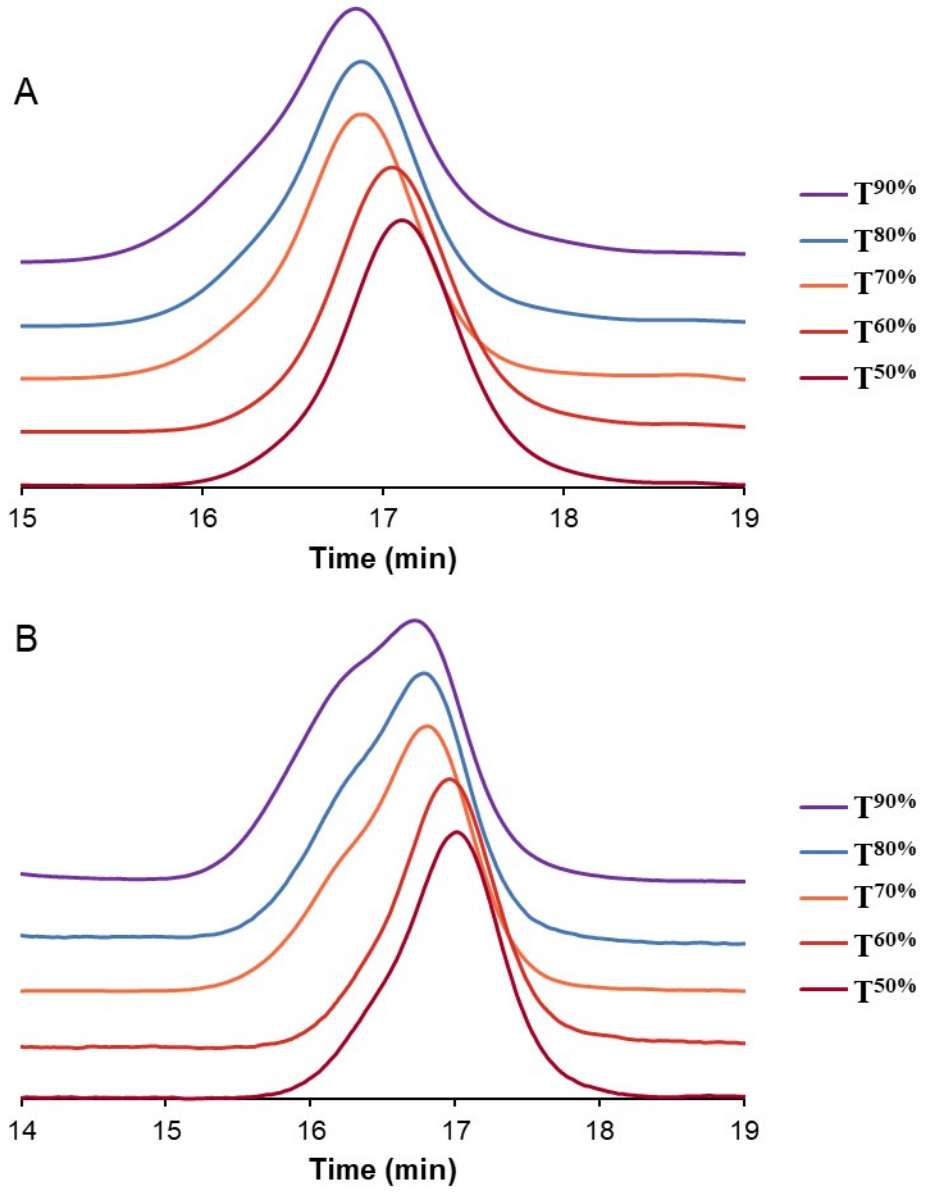

Figure S18. SEC traces showing (A) refractive index detector and (B) light scattering detector of P*t*BA MMs **T$^{50\%}$**, **T$^{60\%}$**, **T$^{70\%}$**, **T$^{80\%}$** and **T$^{90\%}$**.

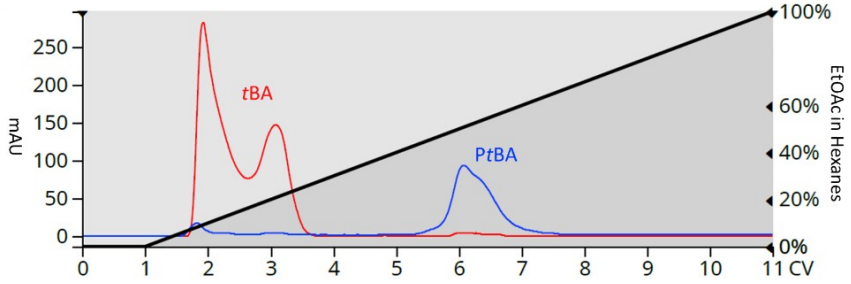

Figure S19. PtBA-MM purification plot showing the absorption of monomer at 265 nm (red) and the MM at 305 nm (blue) as the polarity of the mobile phase increases.

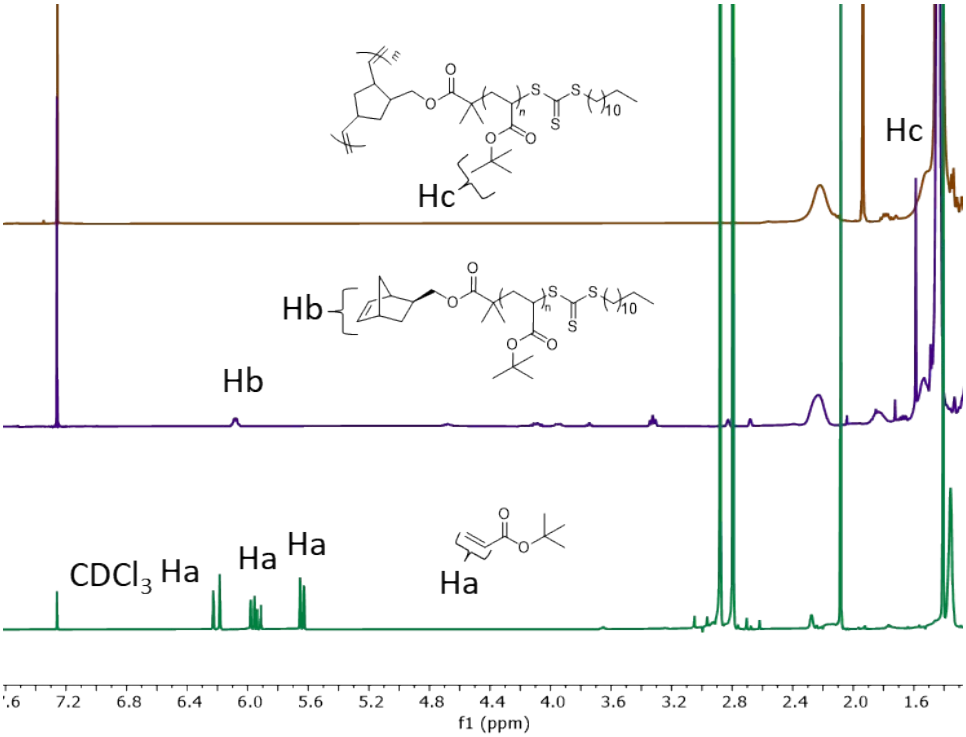

Figure S20. ^{1}H NMR stacked spectra showing the progress of $T_{100}^{50\%}$ from crude MM containing unreacted monomer after RAFT polymerization (bottom) to purified PtBA-MM after silica column (middle) and to PtBA-BB after ROMP (top).

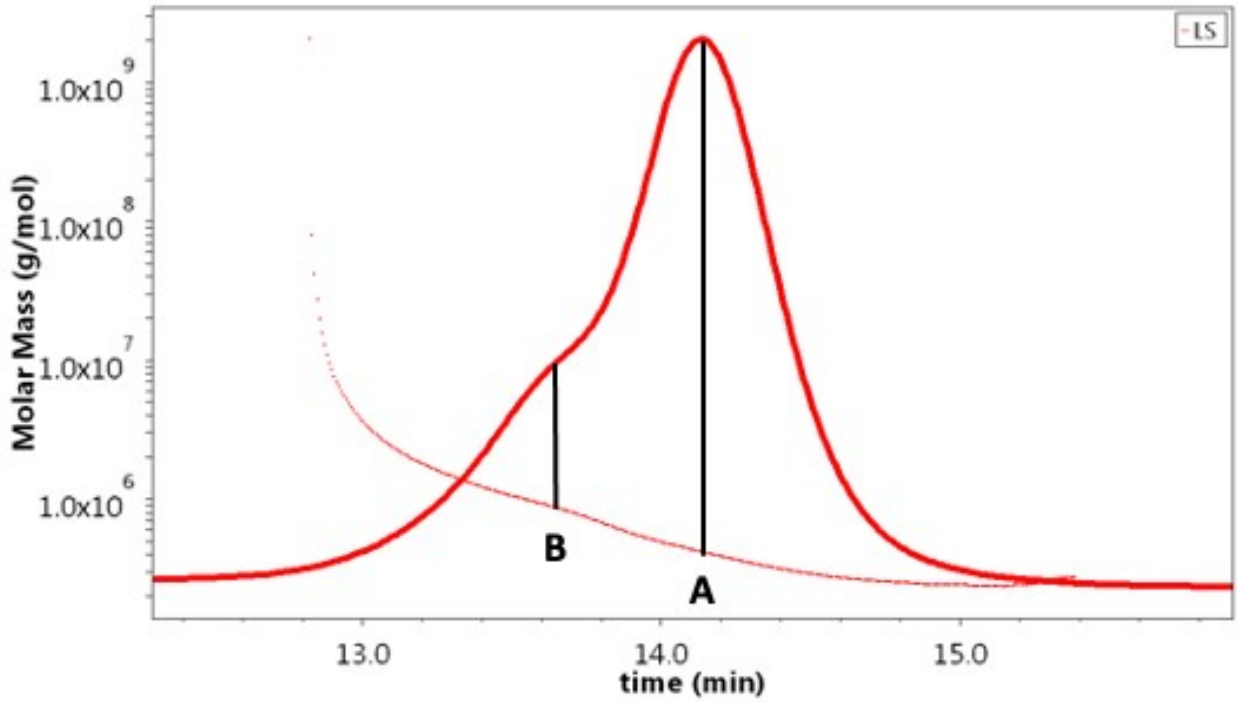

Figure S21. SEC trace of light scattering detector and molar mass of bottlebrush polymer $T_{100}^{80\%}$. The molar mass of peak A is 413 kg/mol and peak B is 848 kg/mol.

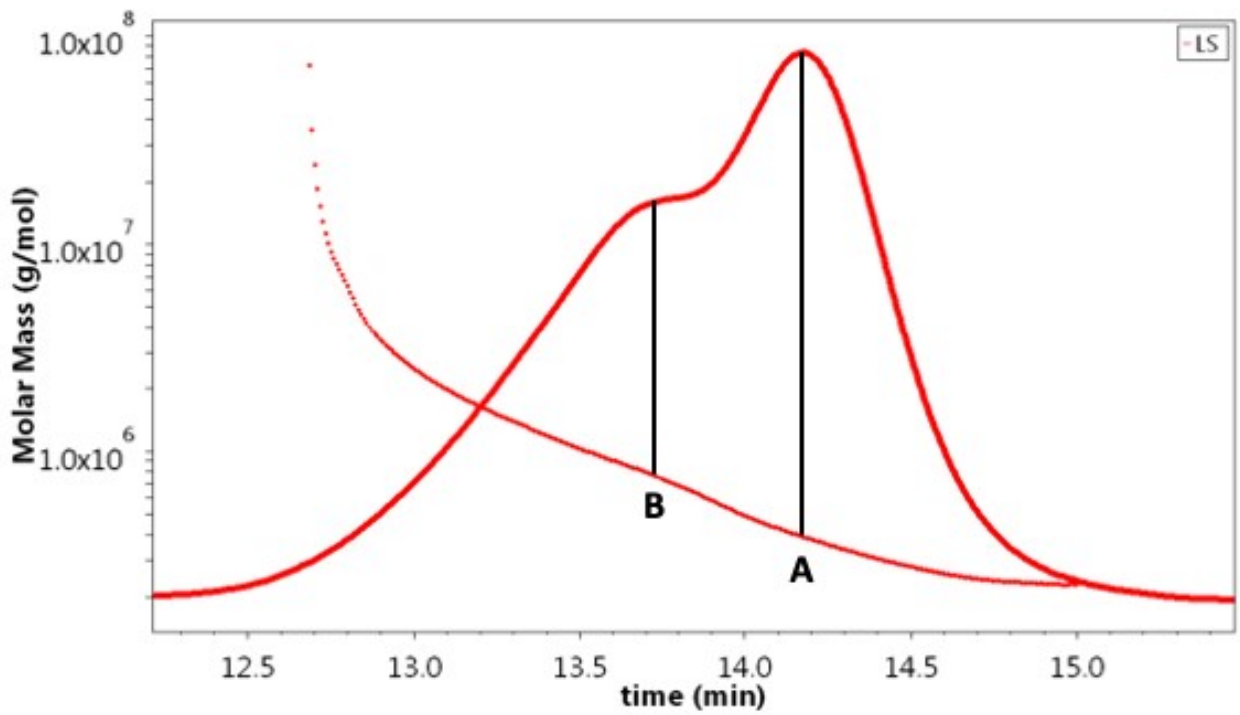

Figure S22. SEC trace of light scattering detector and molar mass of bottlebrush polymer $T_{100}^{90\%}$. The molar mass of peak A is 396 kg/mol and peak B is 888 kg/mol.

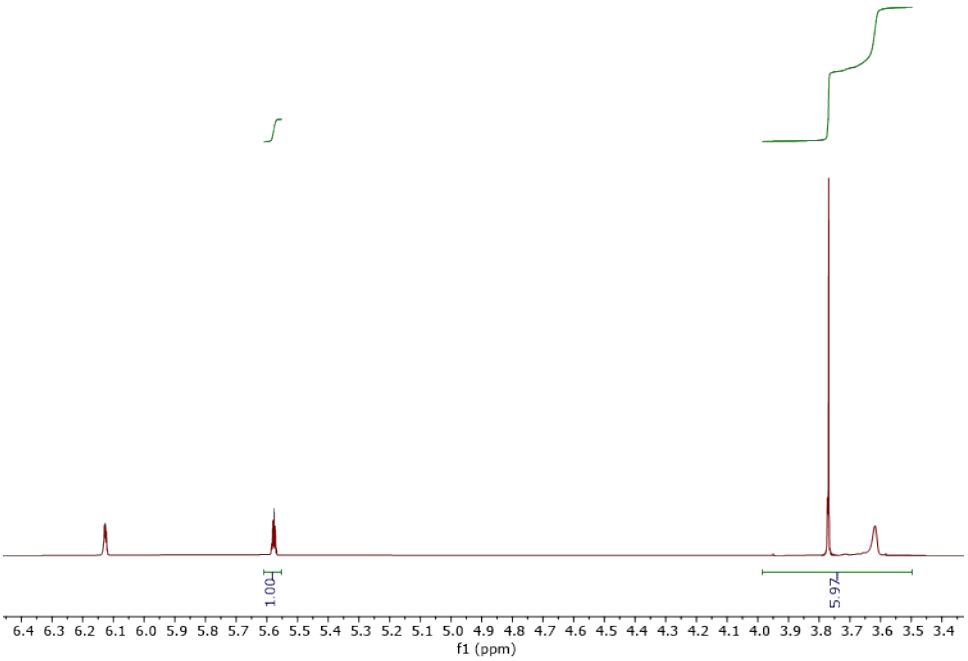

Figure S23. ^{1}H NMR spectrum showing crude aliquot of $\mathbf{M}^{50\%}$ containing unreacted monomer and MM after RAFT polymerization reaching a monomer conversion of 50%.

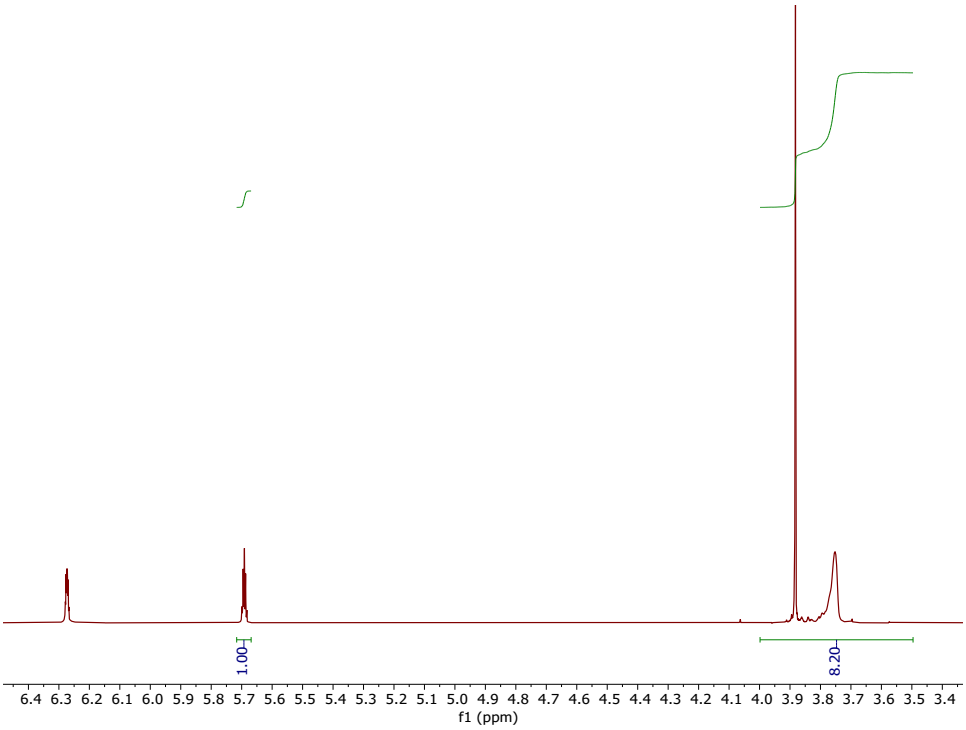

Figure S24. ^{1}H NMR spectrum showing crude aliquot of $\mathbf{M}^{60\%}$ containing unreacted monomer and MM after RAFT polymerization reaching a monomer conversion of 63%.

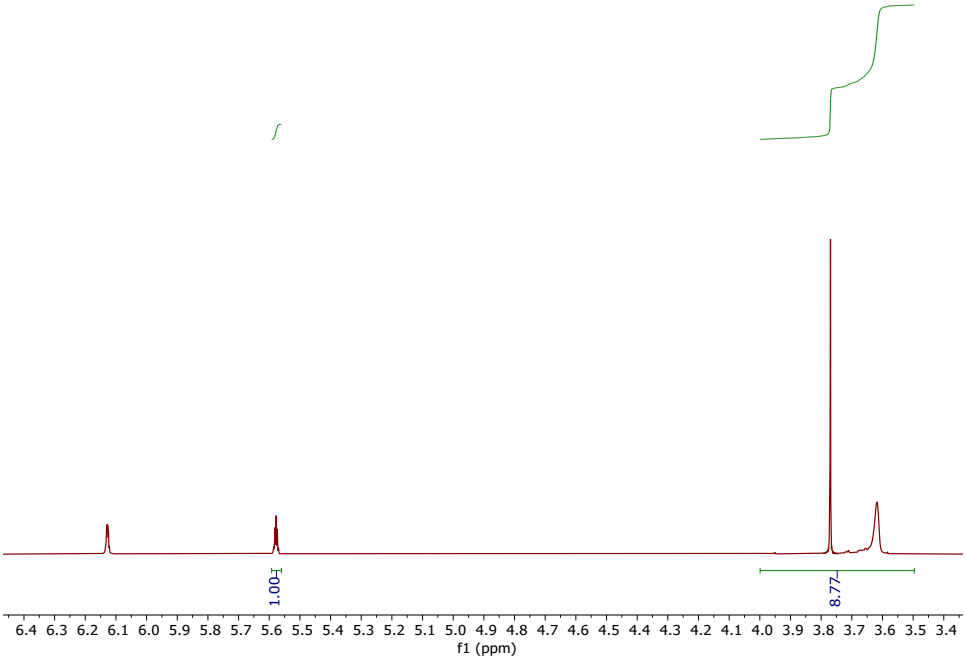

Figure S25. ^{1}H NMR spectrum showing crude aliquot of $\mathbf{M}^{70\%}$ containing unreacted monomer and MM after RAFT polymerization reaching a monomer conversion of 66%.

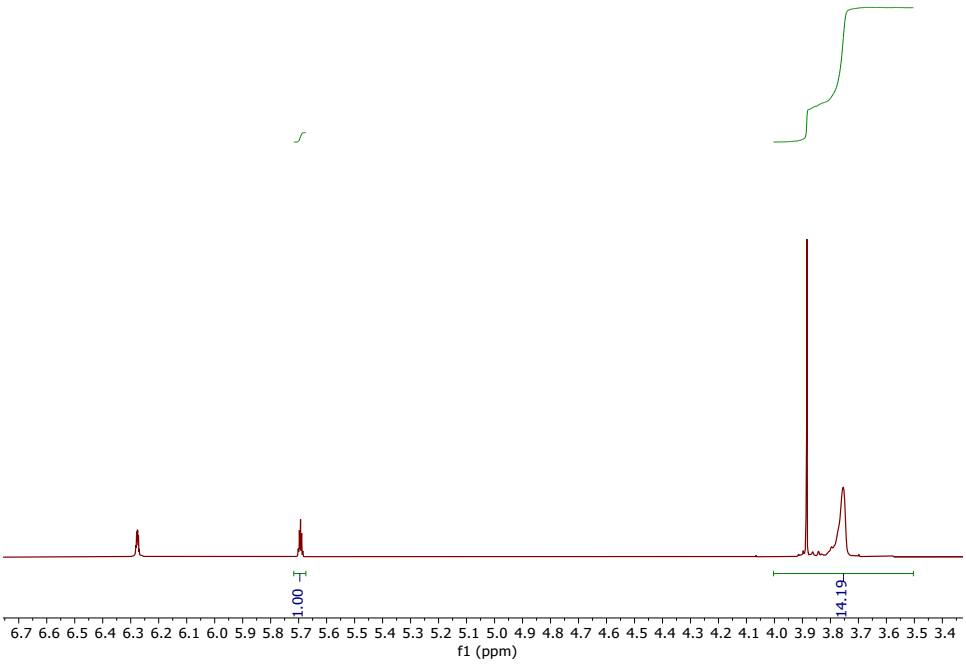

Figure S26. ^{1}H NMR spectrum showing crude aliquot of $\mathbf{M}^{80\%}$ containing unreacted monomer and MM after RAFT polymerization reaching a monomer conversion of 79%.

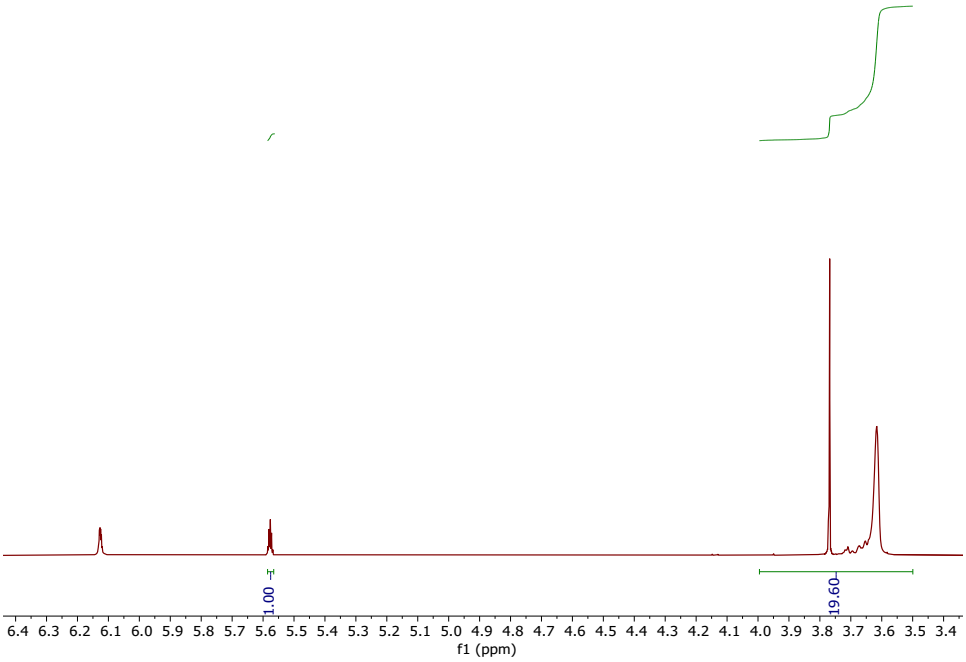

Figure S27. ^{1}H NMR spectrum showing crude aliquot of $\mathbf{M}^{90\%}$ containing unreacted monomer and MM after RAFT polymerization reaching a monomer conversion of 85%.

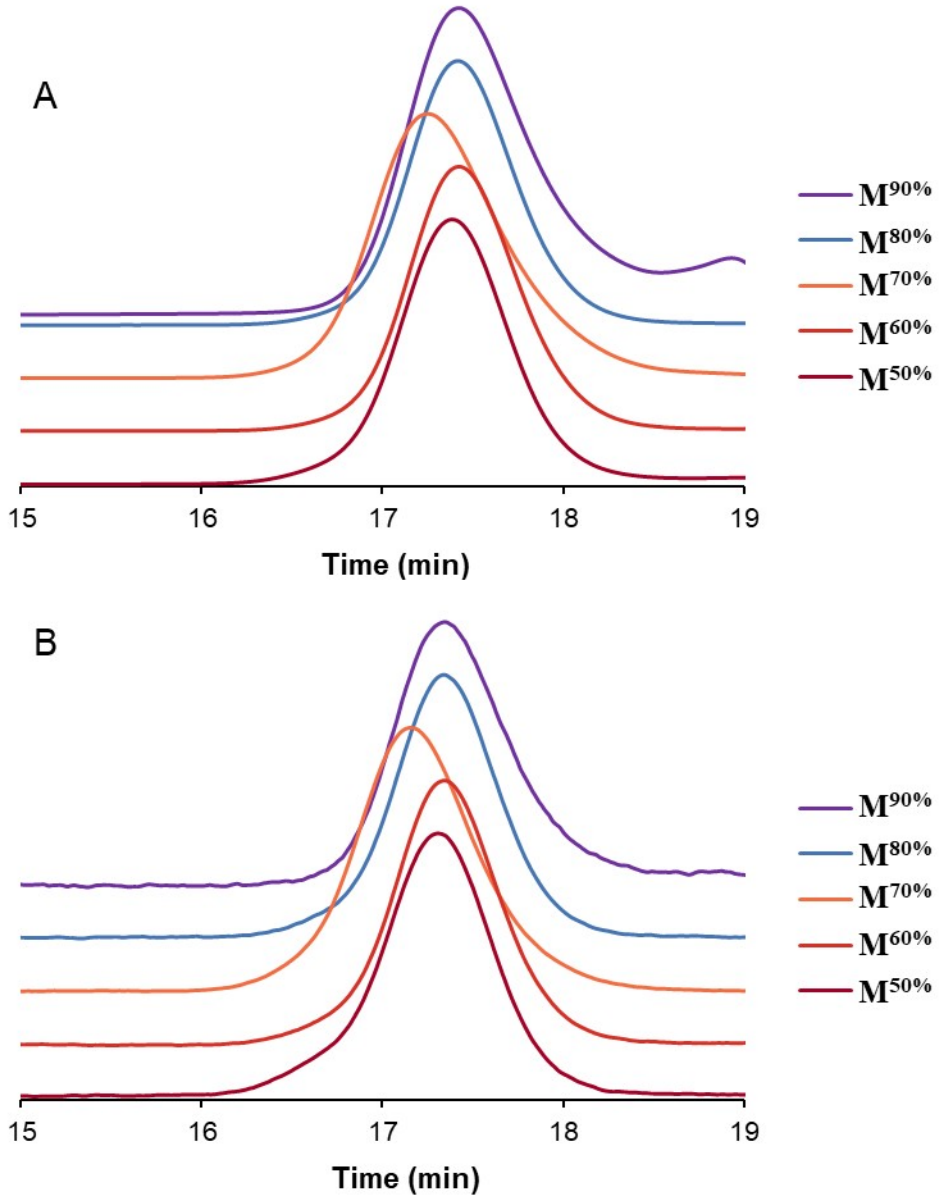

Figure S28. SEC traces showing (A) refractive index detector and (B) light scattering detector of PMMA MMs $\mathbf{M}^{50\%}$, $\mathbf{M}^{60\%}$, $\mathbf{M}^{70\%}$, $\mathbf{M}^{80\%}$ and $\mathbf{M}^{90\%}$.

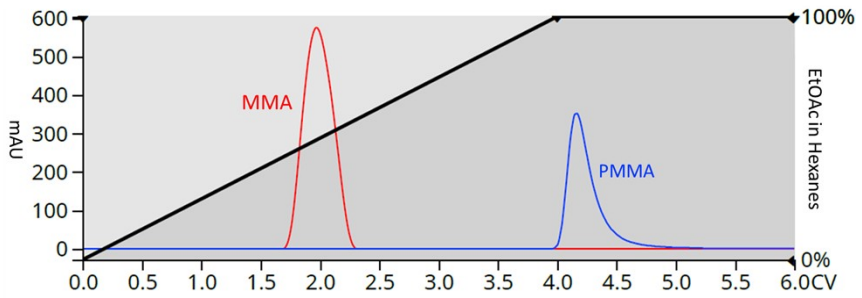

Figure S29. PMMA-MM purification plot showing the absorption of monomer at 253 nm (red) and the MM at 330 nm (blue) as the polarity of the mobile phase increases.

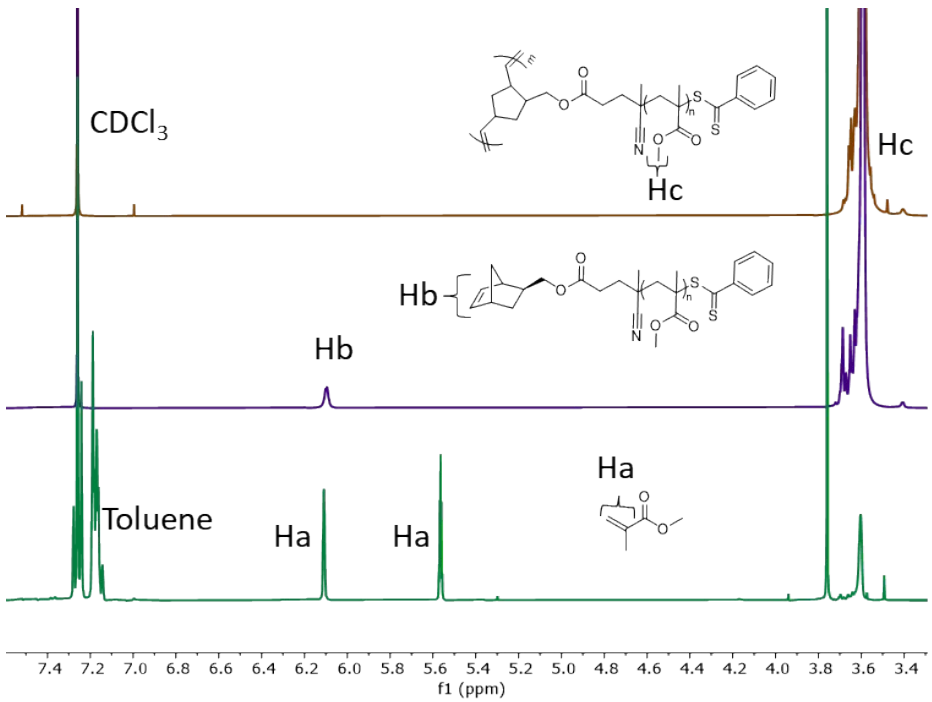

Figure S30. ^{1}H NMR stacked spectra showing the progress of $M_{100}^{50\%}$ from crude MM containing unreacted monomer after RAFT polymerization (bottom) to purified PMMA-MM after silica column (middle) and to PMMA-BB after ROMP (top).

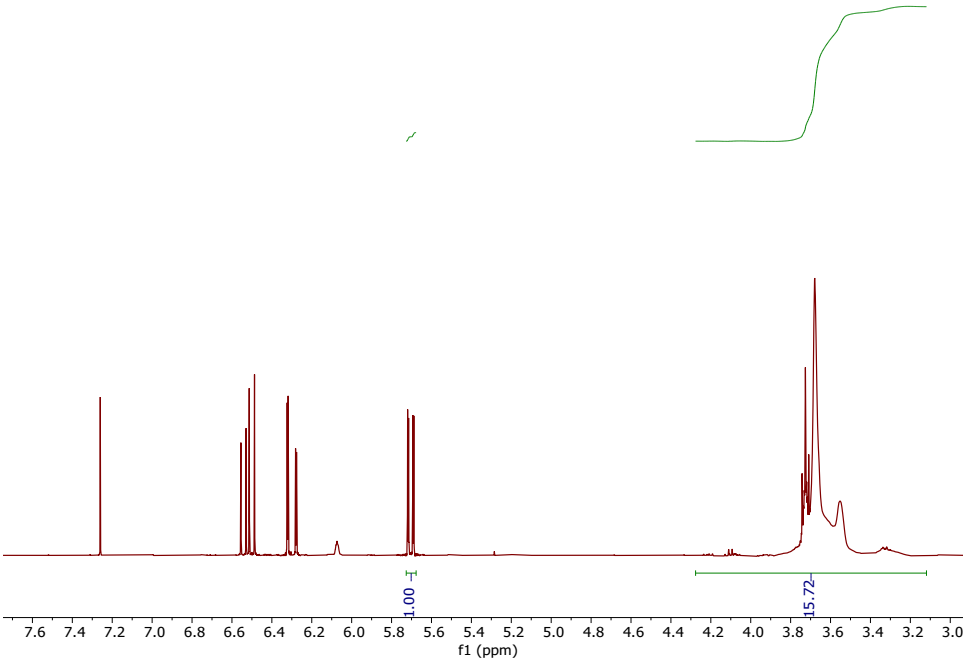

Figure S31. ^{1}H NMR spectrum showing crude aliquot of $\mathbf{A}^{50\%}$ containing unreacted monomer and MM after RAFT polymerization reaching a monomer conversion of 49%.

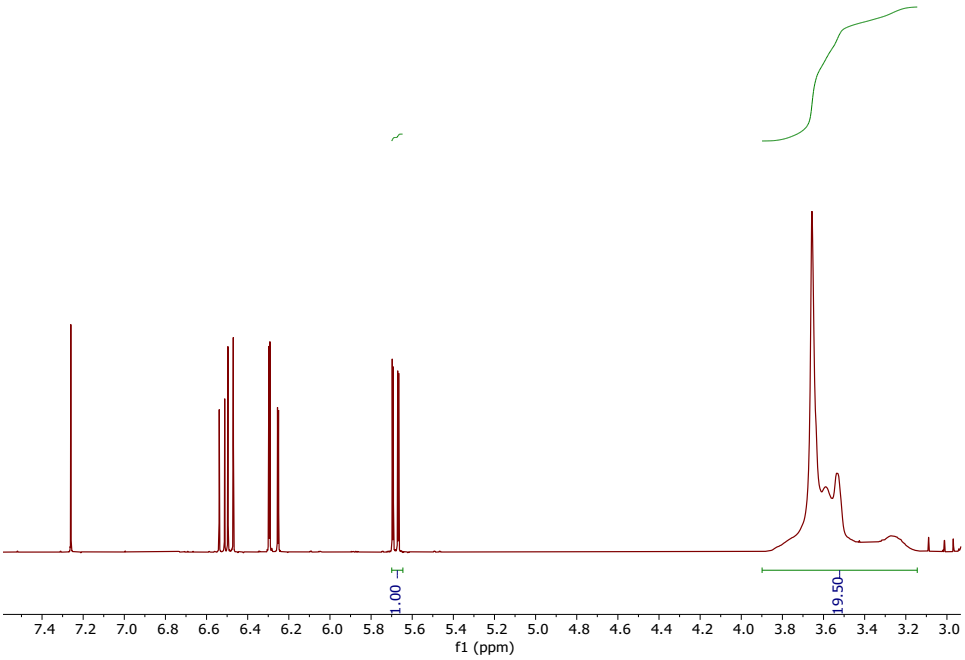

Figure S32. ^{1}H NMR spectrum showing crude aliquot of $\mathbf{A}^{60\%}$ containing unreacted monomer and MM after RAFT polymerization reaching a monomer conversion of 59%.

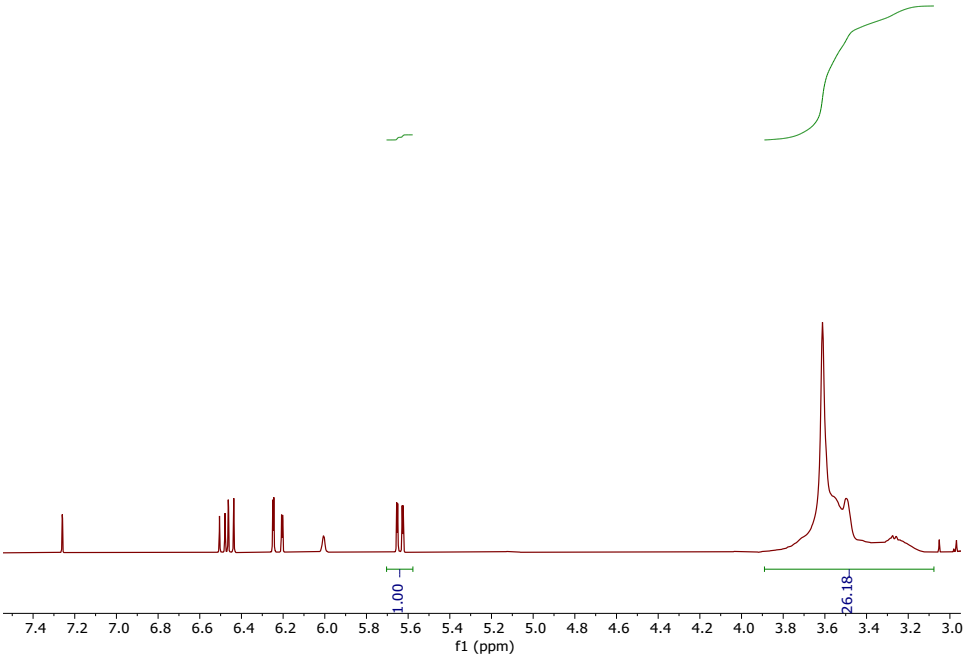

Figure S33. ^{1}H NMR spectrum showing crude aliquot of $\mathbf{A}^{70\%}$ containing unreacted monomer and MM after RAFT polymerization reaching a monomer conversion of 70%.

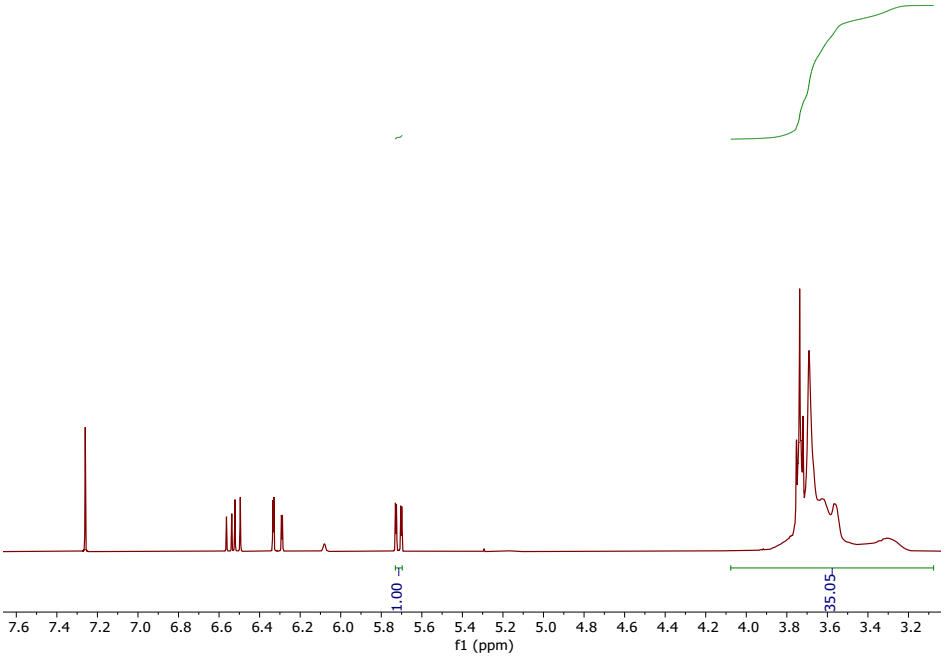

Figure S34. ^{1}H NMR spectrum showing crude aliquot of $\mathbf{A}^{80\%}$ containing unreacted monomer and MM after RAFT polymerization reaching a monomer conversion of 77%.

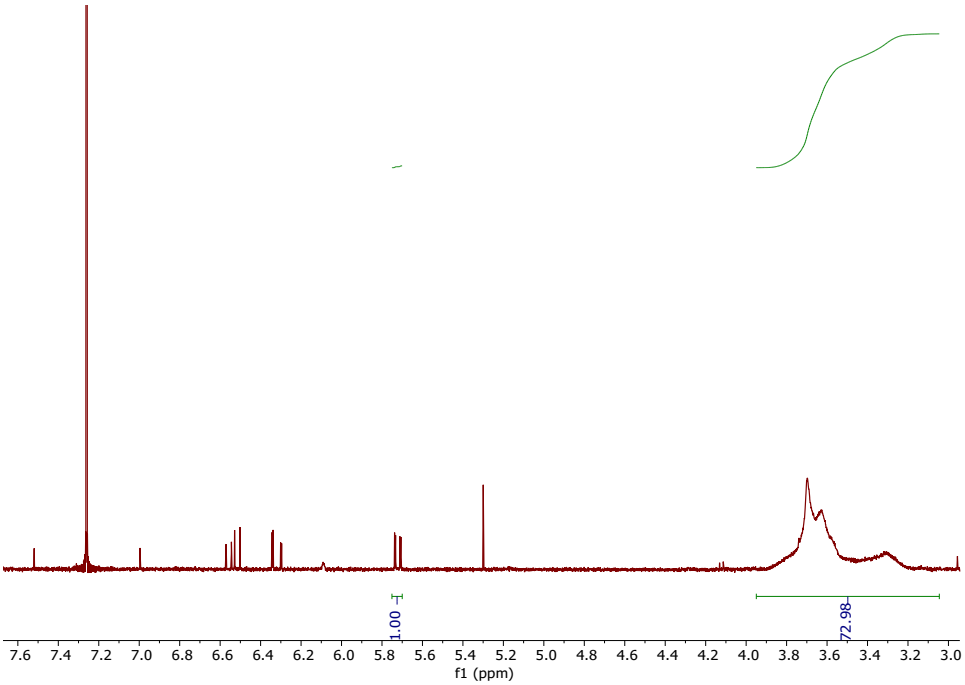

Figure S35. ^{1}H NMR spectrum showing crude aliquot of $\mathbf{A}^{90\%}$ containing unreacted monomer and MM after RAFT polymerization reaching a monomer conversion of 89%.

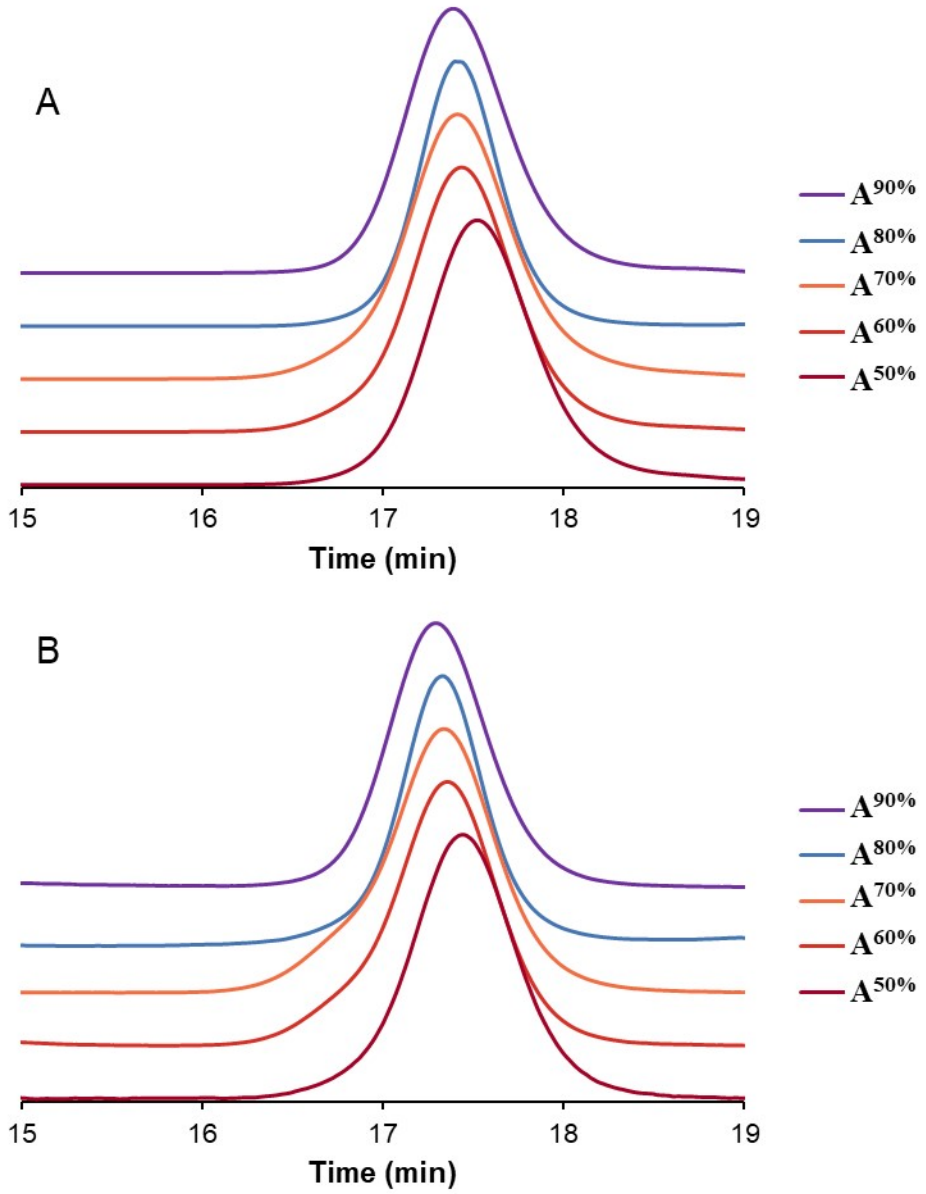

Figure S36. SEC traces showing (A) refractive index detector and (B) light scattering detector of PACMO MMs $\mathbf{A}^{50\%}$, $\mathbf{A}^{60\%}$, $\mathbf{A}^{70\%}$, $\mathbf{A}^{80\%}$ and $\mathbf{A}^{90\%}$.

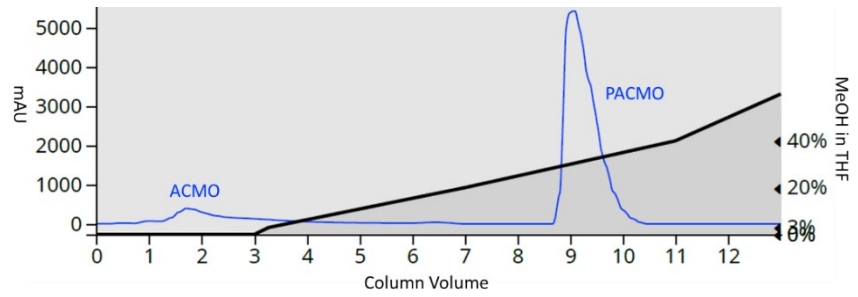

Figure S37. PACMO-MM purification plot showing the absorption of monomer and the MM at 210 nm (blue) as the polarity of the mobile phase increases.

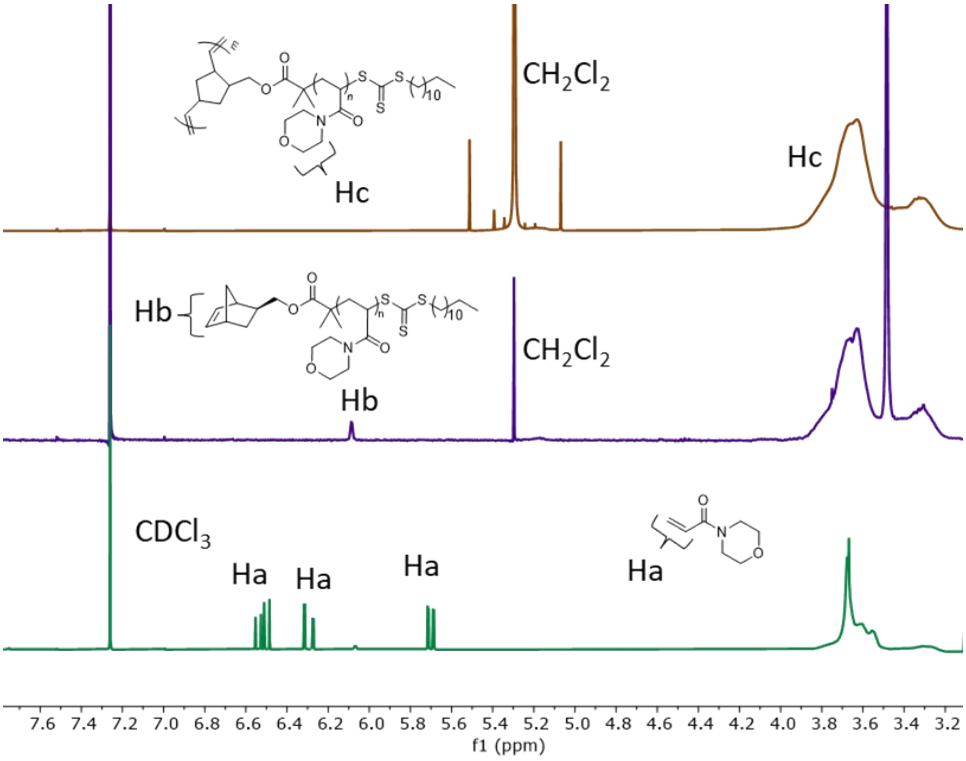

Figure S38. ^{1}H NMR stacked spectra showing the progress of $A_{100}^{80\%}$ from crude MM containing unreacted monomer after RAFT polymerization (bottom) to purified PACMO-MM after silica column (middle) and to PACMO-BB after ROMP (top).

Deconvolution of Coupled Bottlebrush Polymers

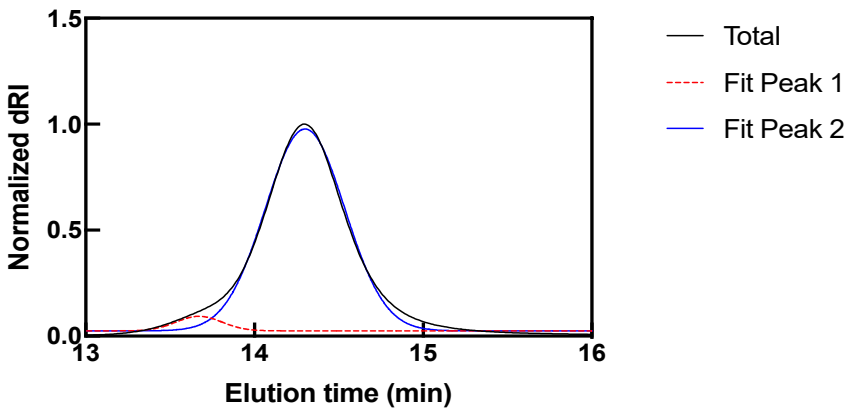

Figure S39. RI signal from SEC of $S_{100}^{20\%}$ (solid, black), deconvoluted coupled bottlebrush products (dash, red), and deconvoluted uncoupled bottlebrush product (dash, blue).

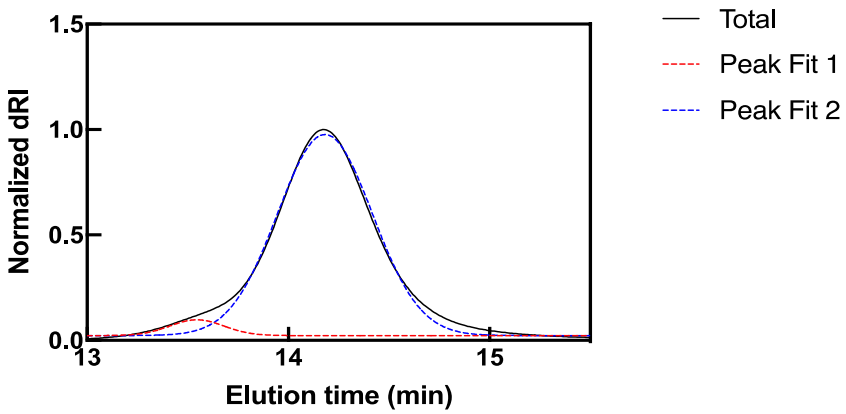

Figure S40. RI signal from SEC of $S_{100}^{30\%}$ (solid, black), deconvoluted coupled bottlebrush products (dash, red), and deconvoluted uncoupled bottlebrush product (dash, blue).

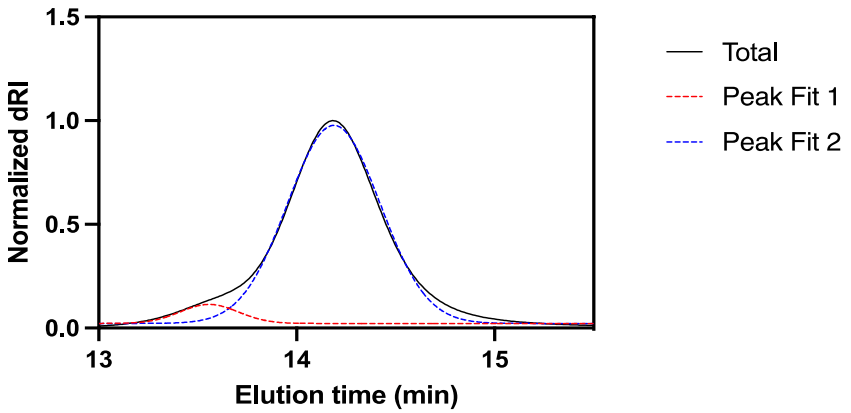

Figure S41. RI signal from SEC of $S_{100}^{40\%}$ (solid, black), deconvoluted coupled bottlebrush products (dash, red), and deconvoluted uncoupled bottlebrush product (dash, blue).

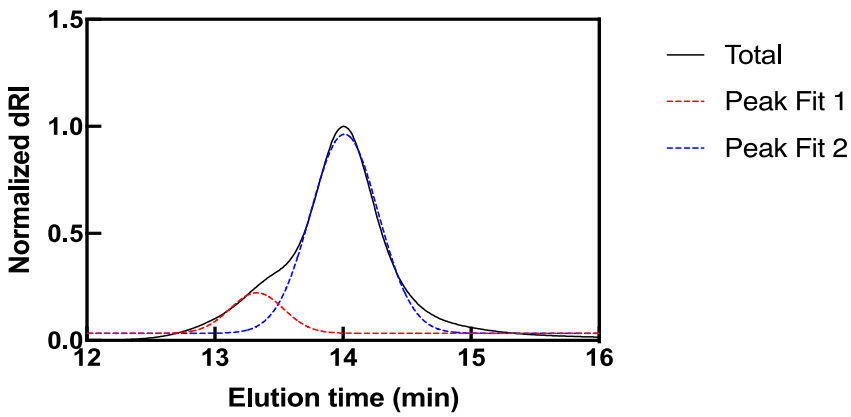

Figure S42. RI signal from SEC of $S_{100}^{50\%}$ (solid, black), deconvoluted coupled bottlebrush products (dash, red), and deconvoluted uncoupled bottlebrush product (dash, blue).

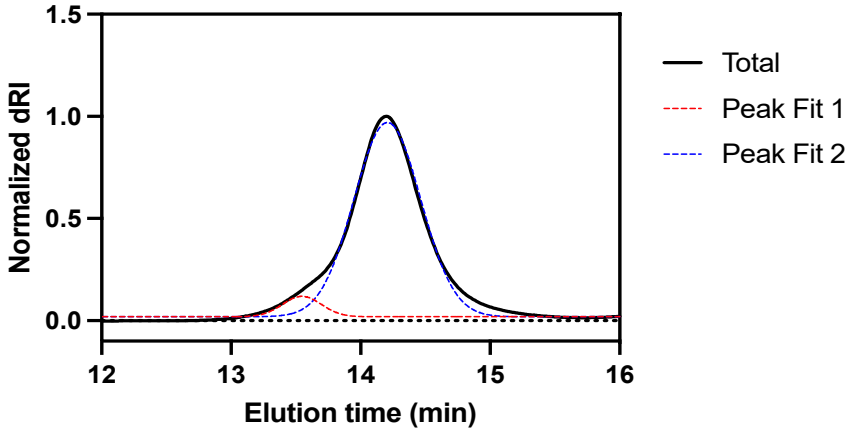

Figure S43. RI signal from SEC of $T_{100}^{80\%}$ (solid, black), deconvoluted coupled bottlebrush products (dash, red), and deconvoluted uncoupled bottlebrush product (dash, blue).

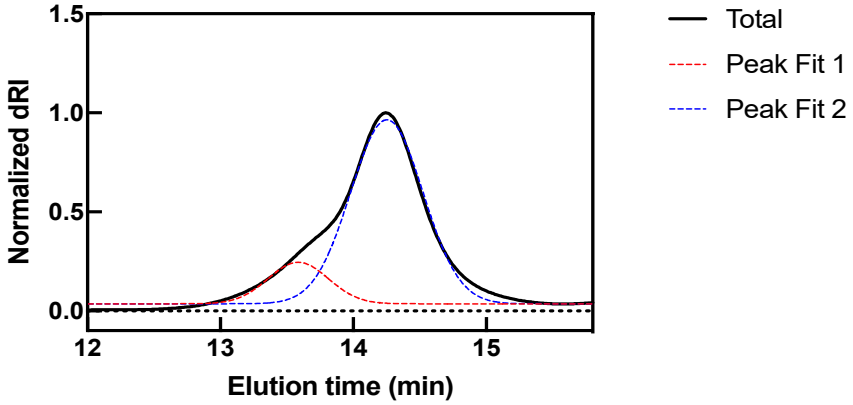

Figure S44. RI signal from SEC of $T_{100}^{90\%}$ (solid, black), deconvoluted coupled bottlebrush products (dash, red), and deconvoluted uncoupled bottlebrush product (dash, blue).

End group Analysis of Macromonomers

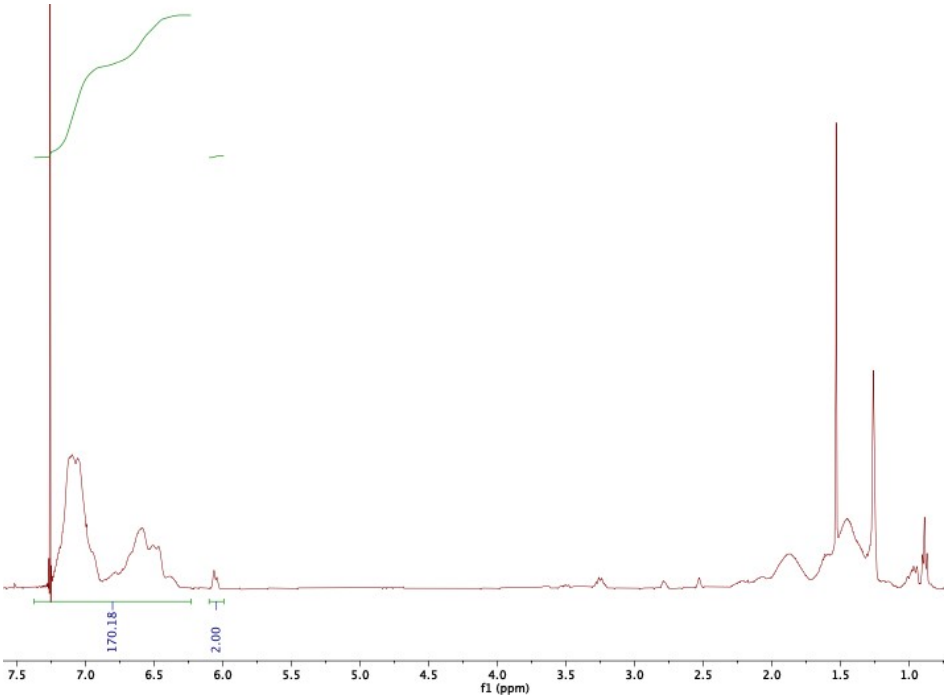

Figure S45. ^{1}H NMR spectrum of $\mathbf{S^{10\%}}$

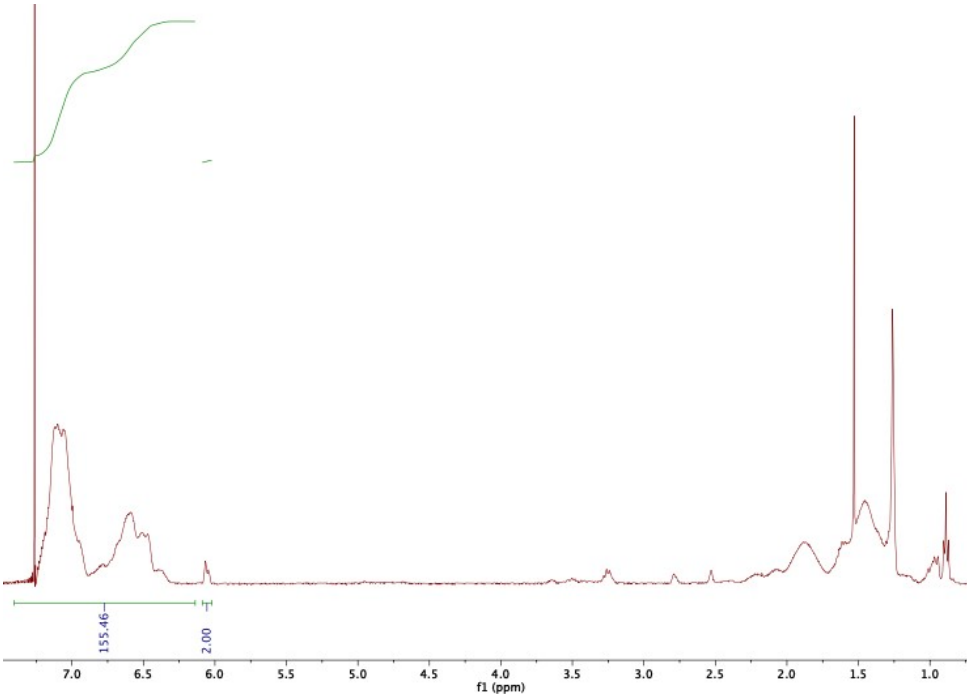

Figure S46. ^{1}H NMR spectrum of $\mathbf{S^{20\%}}$

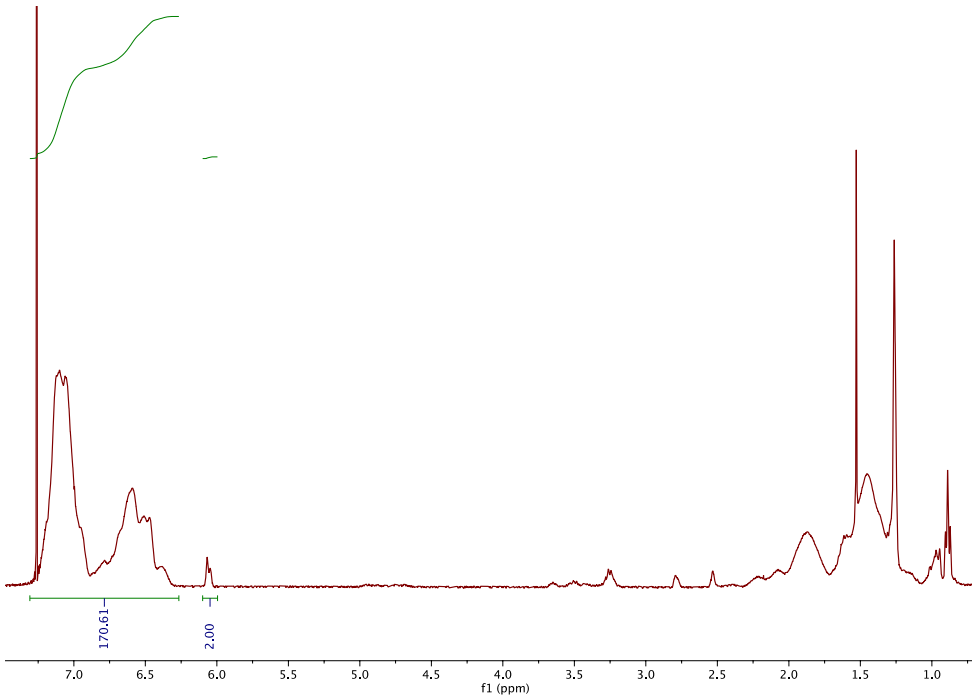

Figure S47. ^{1}H NMR spectrum of $\mathbf{S}^{30\%}$

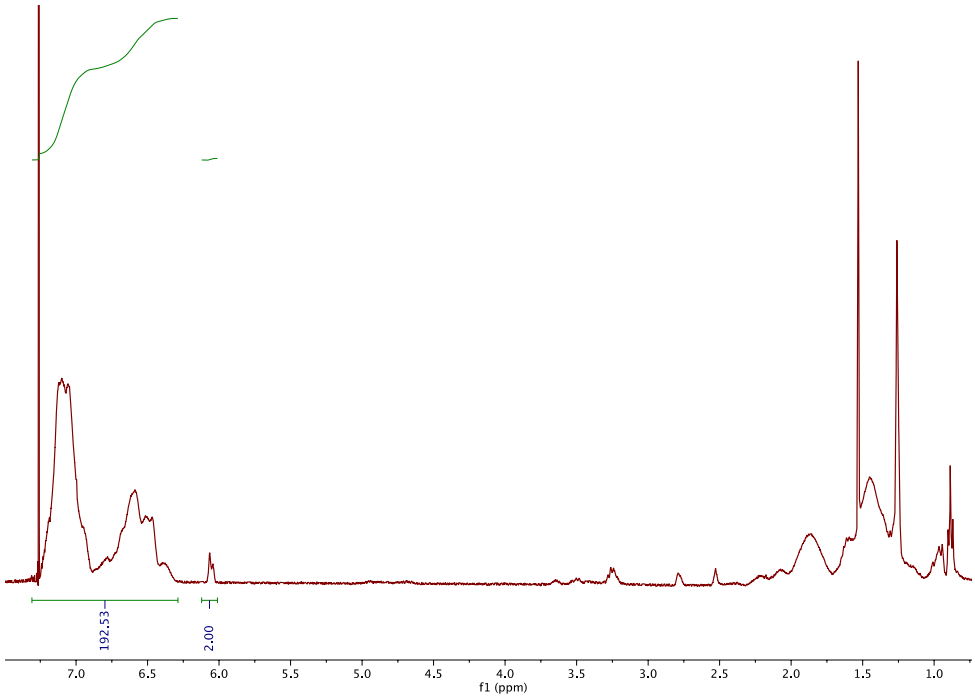

Figure S48. ^{1}H NMR spectrum of $\mathbf{S}^{40\%}$

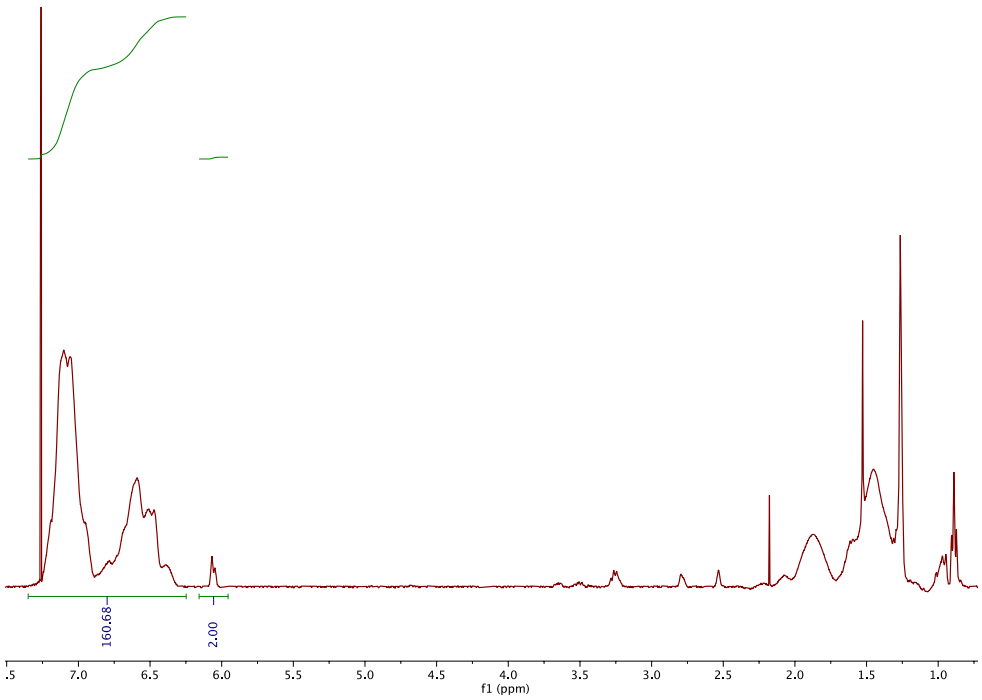

Figure S49. ^{1}H NMR spectrum of **S**$^{50\%}$

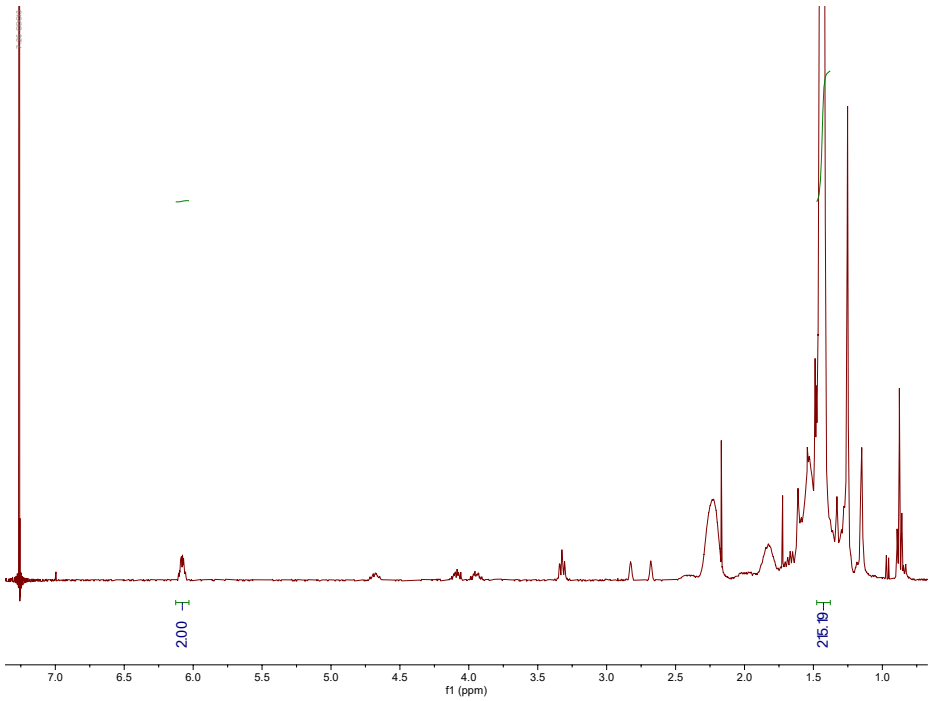

Figure S50. ^{1}H NMR spectrum of **T**$^{50\%}$

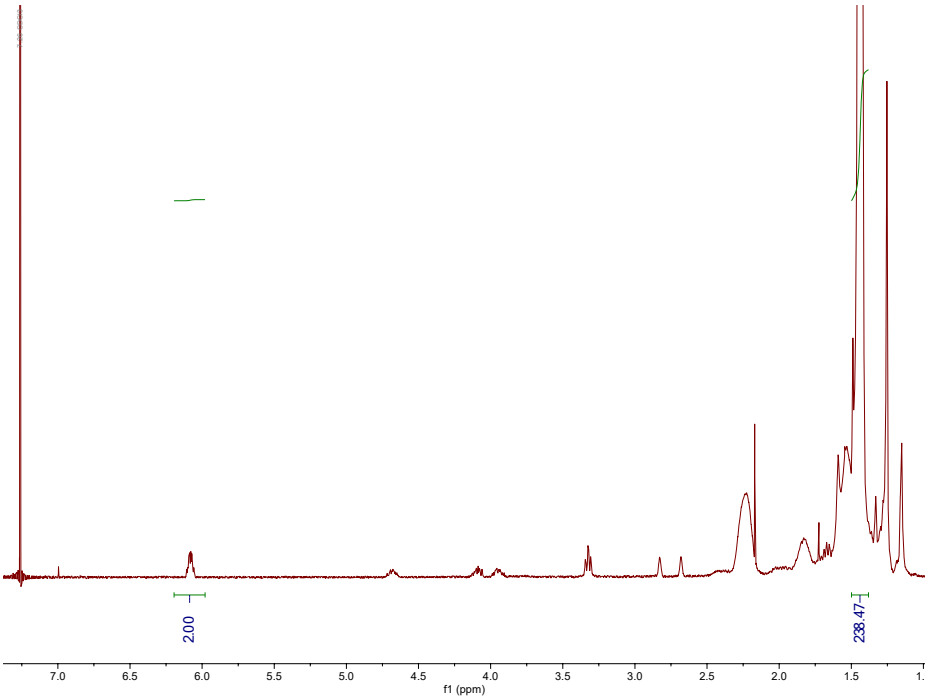

Figure S51. ^{1}H NMR spectrum of $\mathbf{T^{60\%}}$

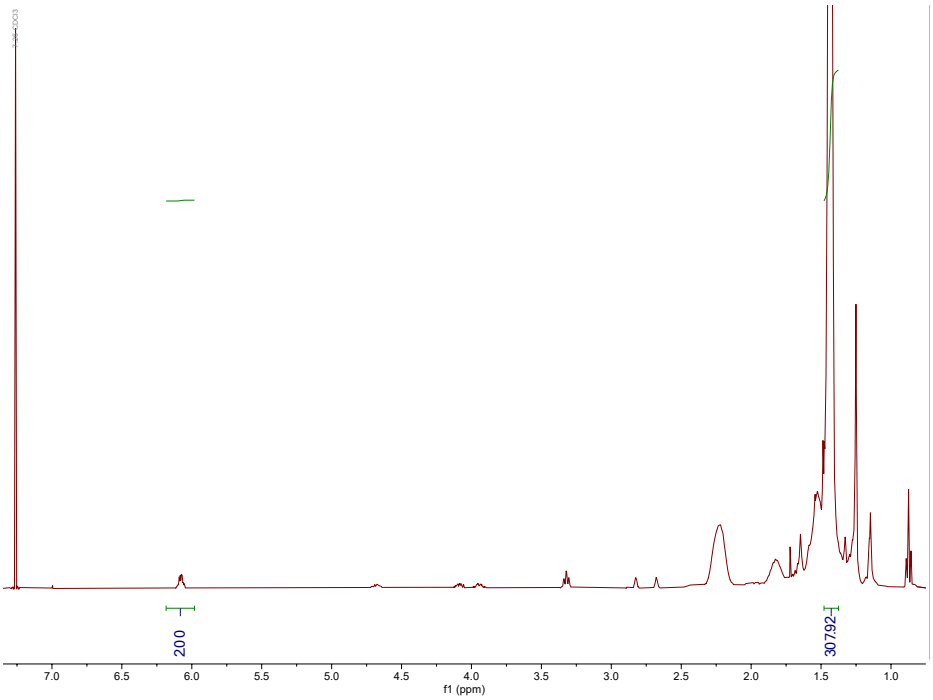

Figure S52. ^{1}H NMR spectrum of $\mathbf{T^{70\%}}$

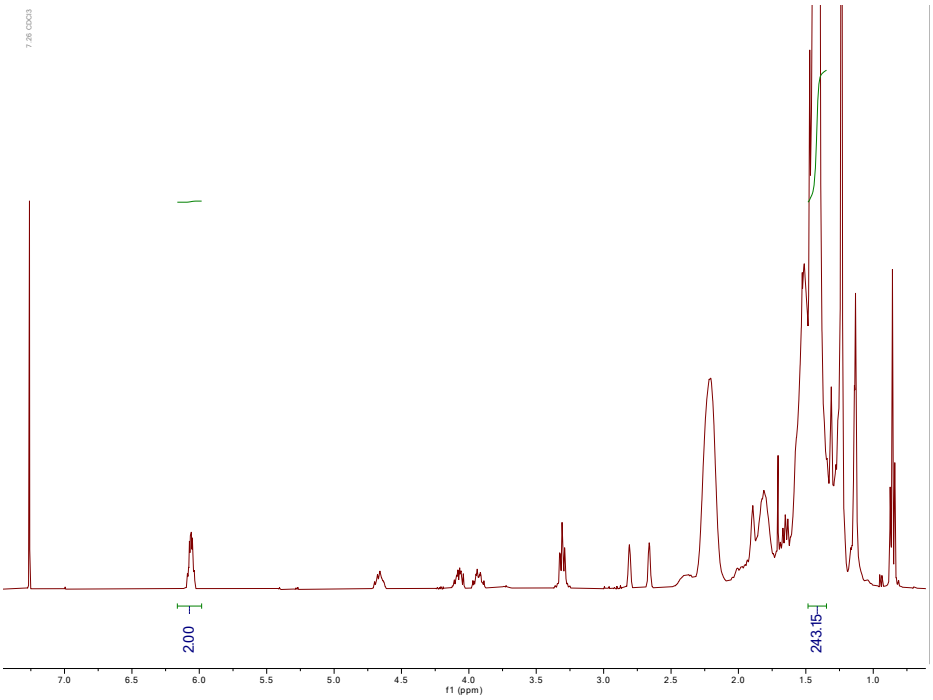

Figure S53. ^{1}H NMR spectrum of $\mathbf{T^{80\%}}$

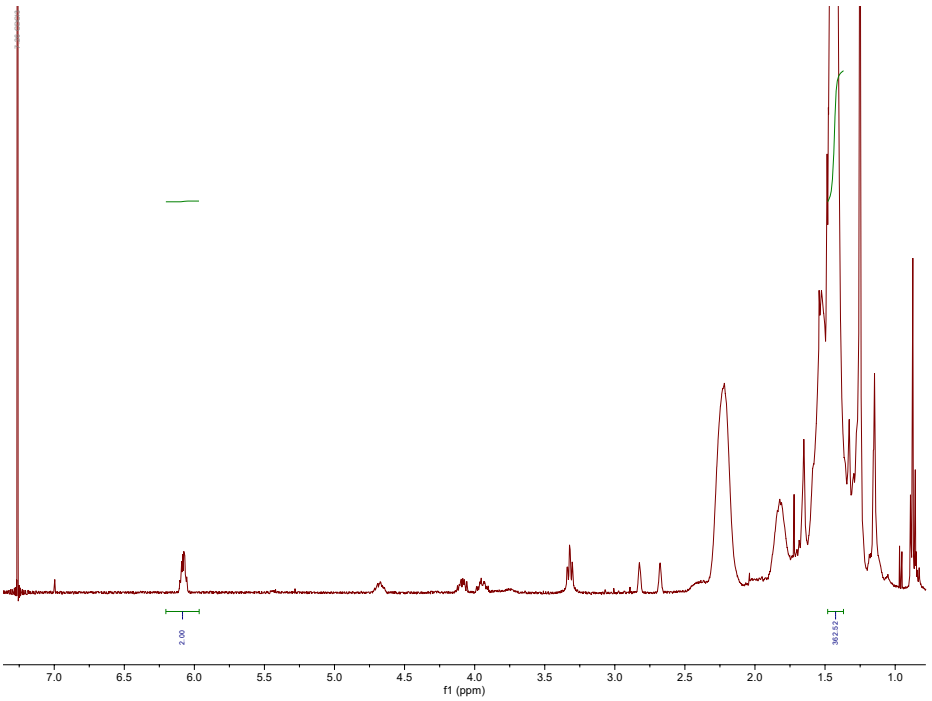

Figure S54. ^{1}H NMR spectrum of $\mathbf{T^{90\%}}$

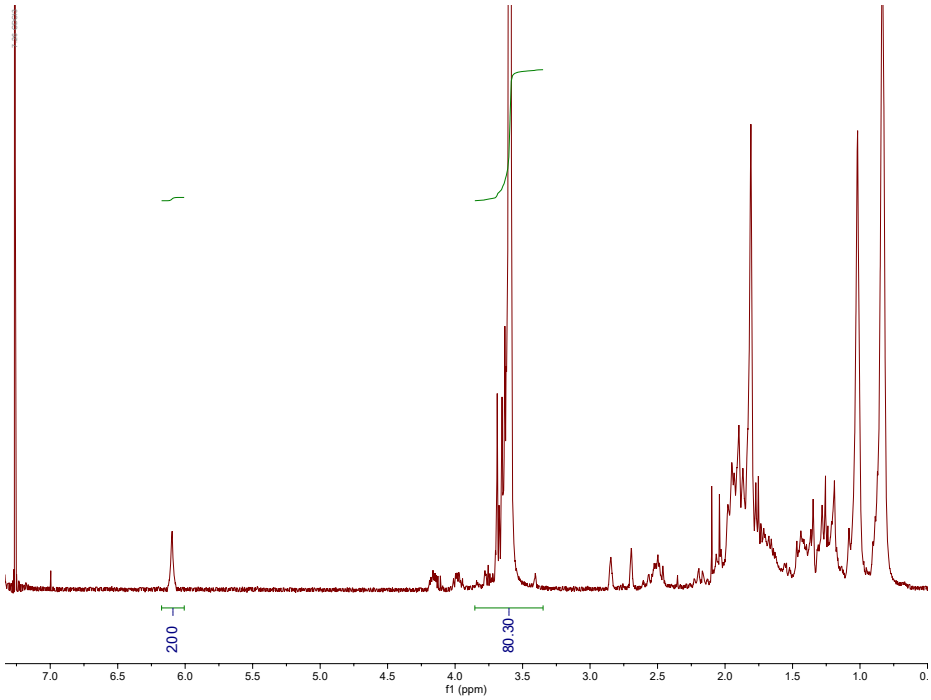

Figure S55. ^{1}H NMR spectrum of **M**$^{50\%}$

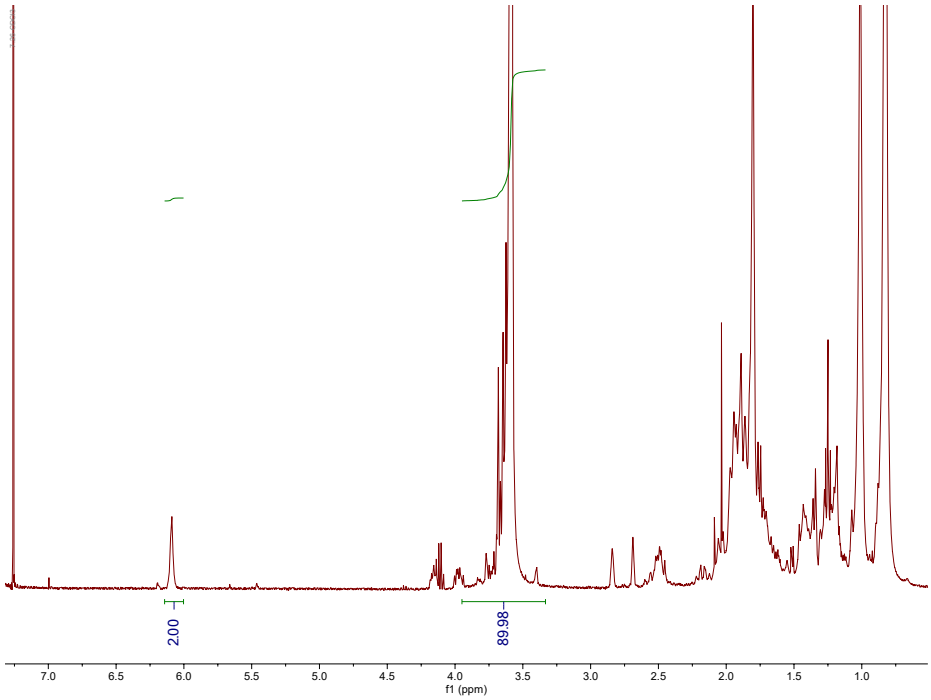

Figure S56. ^{1}H NMR spectrum of **M**$^{60\%}$

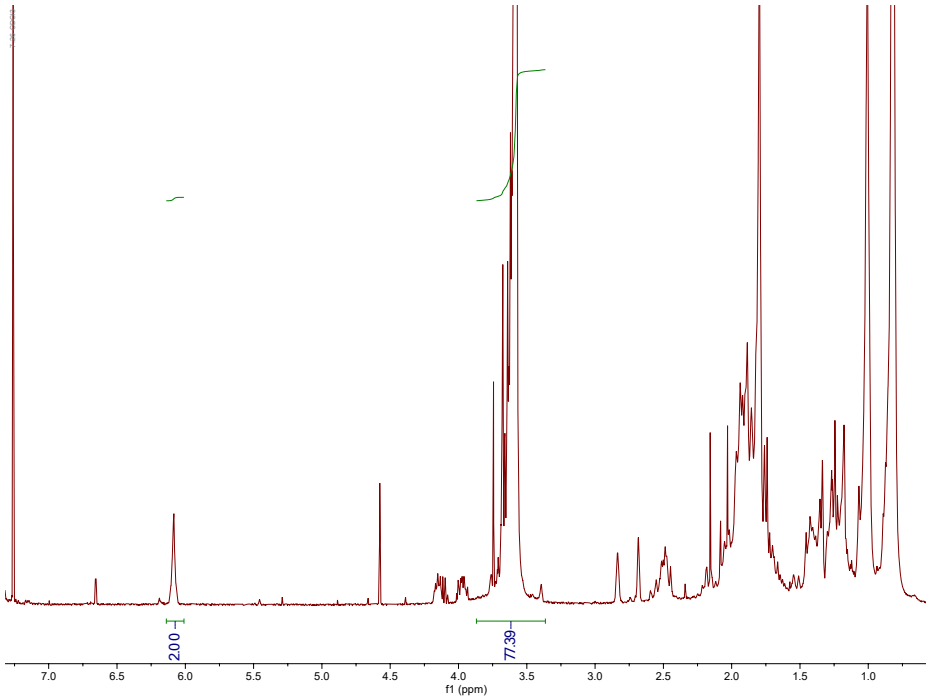

Figure S57. ^{1}H NMR spectrum of $\mathbf{M}^{70\%}$

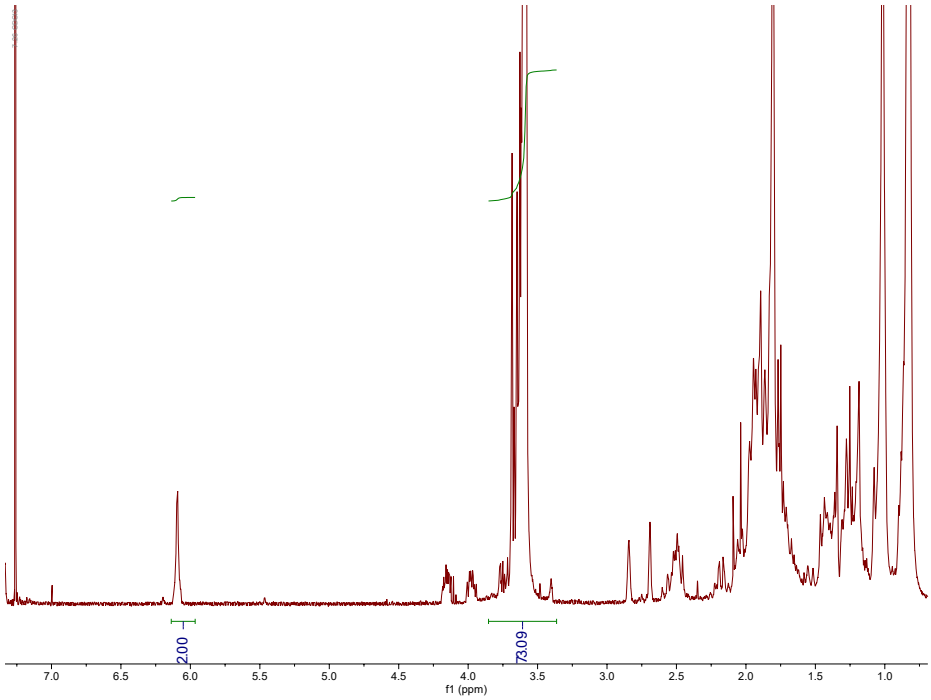

Figure S58. ^{1}H NMR spectrum of $\mathbf{M}^{80\%}$

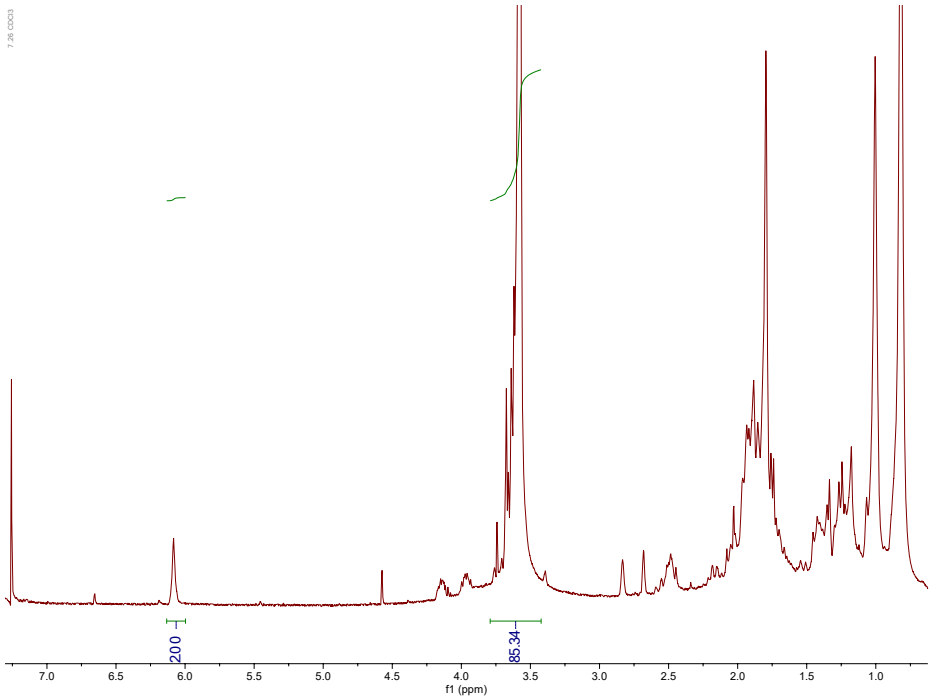

Figure S59. ^{1}H NMR spectrum of $\mathbf{M}^{90\%}$

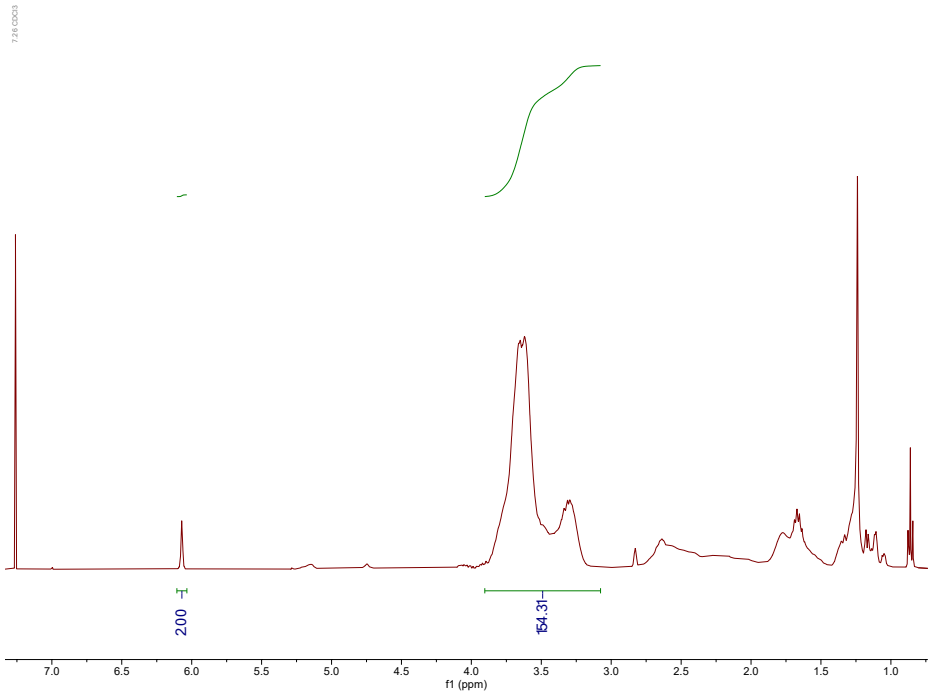

Figure S60. ^{1}H NMR spectrum of $\mathbf{A}^{50\%}$

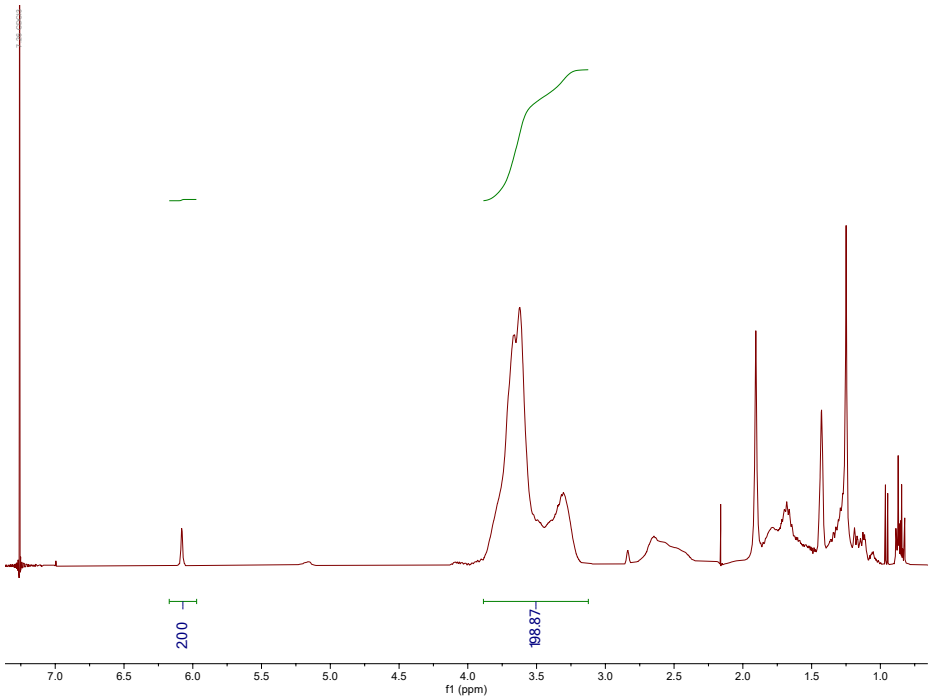

Figure S61. ^{1}H NMR spectrum of $\mathbf{A}^{60\%}$

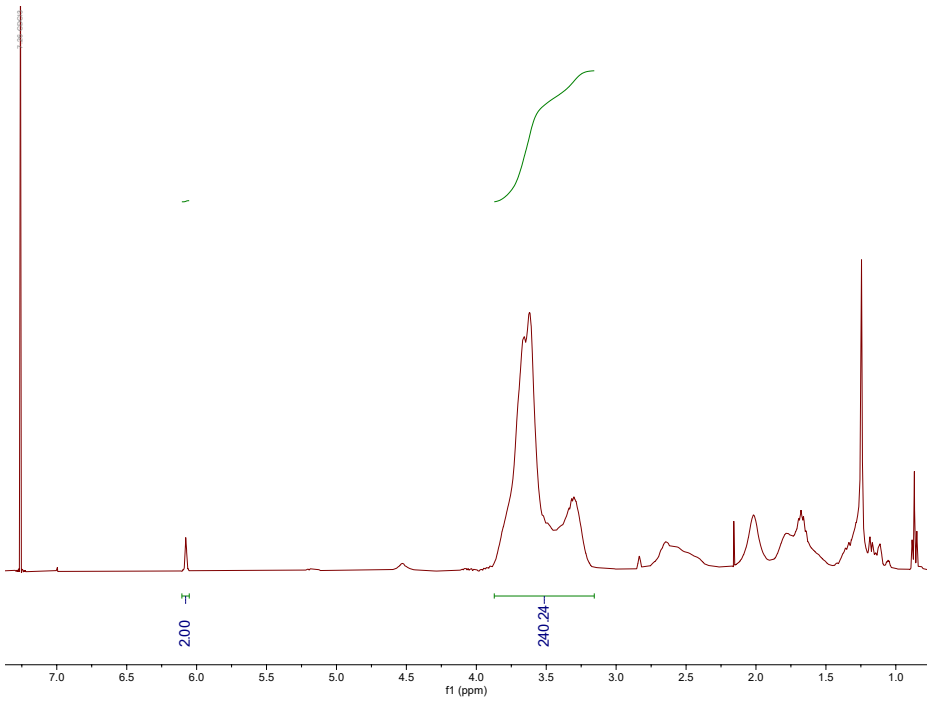

Figure S62. ^{1}H NMR spectrum of $\mathbf{A}^{70\%}$

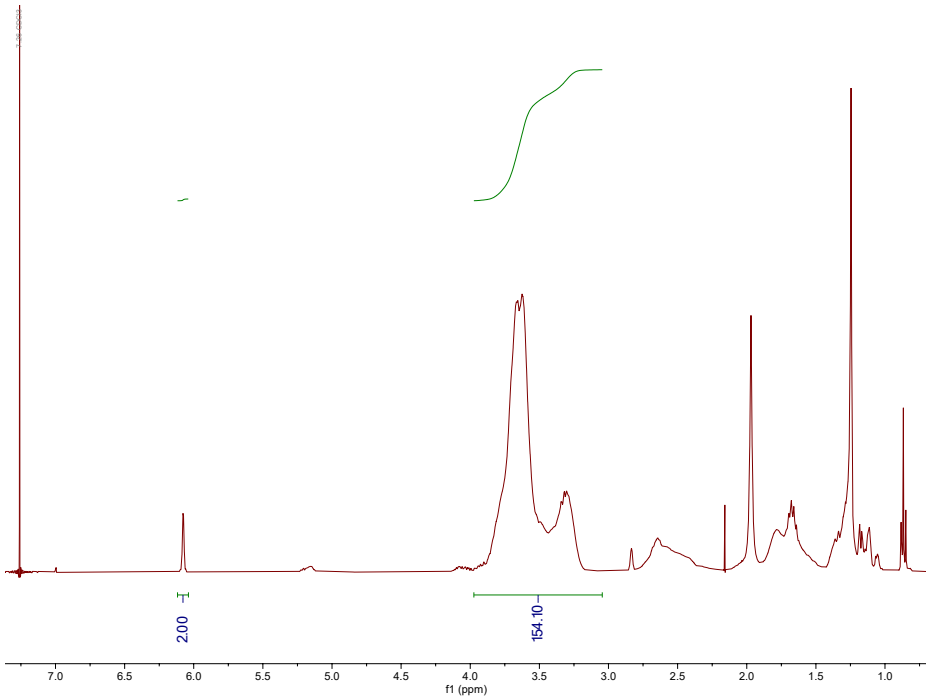

Figure S63. ^{1}H NMR spectrum of $\mathbf{A}^{80\%}$

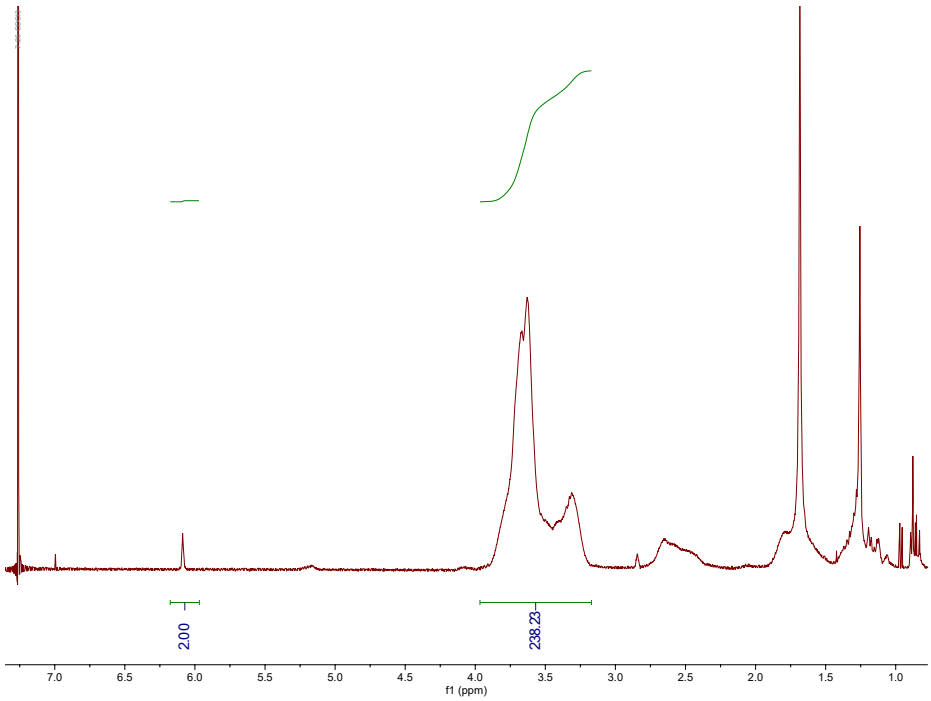

Figure S64. ^{1}H NMR spectrum of $\mathbf{A}^{90\%}$

Offline Measurement of dn/dc of PtBA in THF from RI

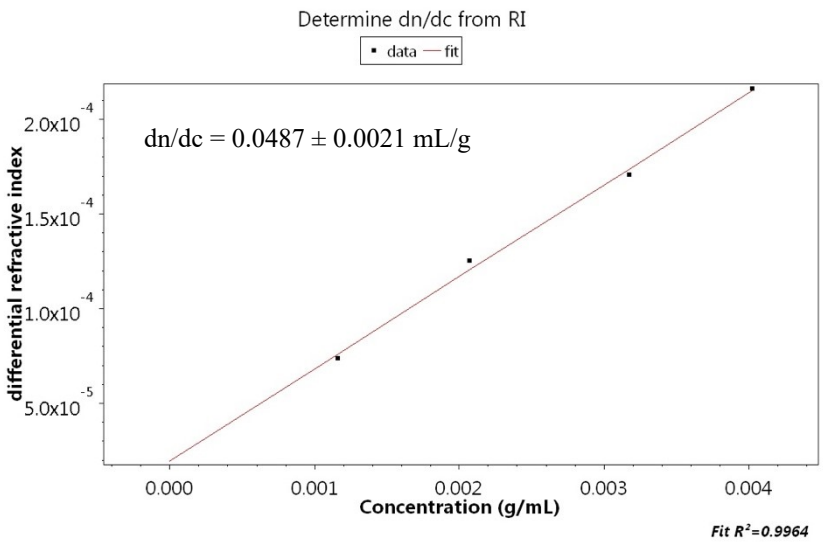

Figure S65. Plot of differential refractive index vs. concentration for PtBA (4 kg/mol made by RAFT using CTA shown in Scheme 2A) in THF at 26 °C.

Offline Measurement of dn/dc of PACMO in THF from RI

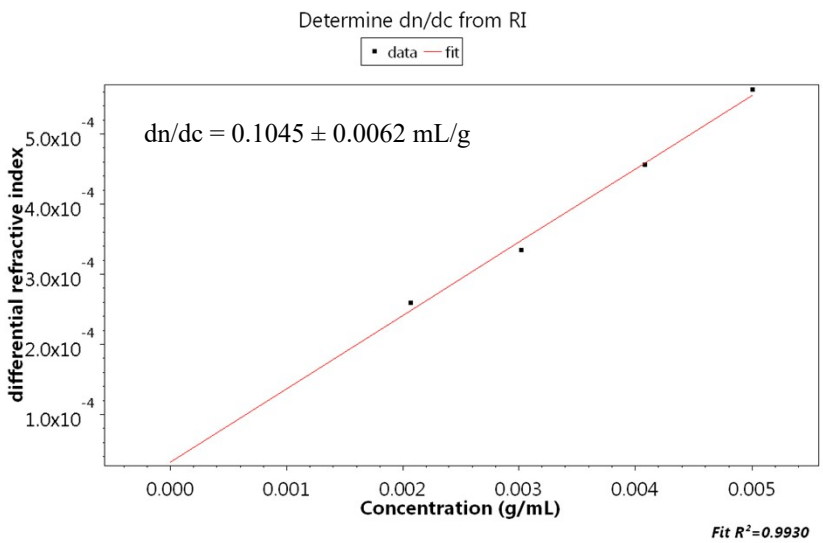

Figure S66. Plot of differential refractive index vs. concentration for PACMO (3 kg/mol made by RAFT using CTA shown in Scheme 2A) in THF at 26 °C.

Table S1. MMs used in this study

MM	$M_{n,theo}$[a] (kg/mol)	$M_{n,NMR}$[b] (kg/mol)	$M_{n,SEC}$[c] (kg/mol)	*Đ*	MM	$M_{n,theo}$[a] (kg/mol)	$M_{n,NMR}$[b] (kg/mol)	$M_{n,SEC}$[c] (kg/mol)	*Đ*
$\mathbf{S}^{10\%}$	3.0	3.5	3.0	1.09	$\mathbf{M}^{50\%}$	3.0	2.7	2.8	1.10
$\mathbf{S}^{20\%}$	2.9	3.2	2.8	1.10	$\mathbf{M}^{60\%}$	3.1	3.0	3.0	1.16
$\mathbf{S}^{30\%}$	3.0	4.5	2.8	1.09	$\mathbf{M}^{70\%}$	2.8	2.6	2.8	1.10
$\mathbf{S}^{40\%}$	3.0	4.0	2.8	1.09	$\mathbf{M}^{80\%}$	2.9	2.8	2.8	1.09
$\mathbf{S}^{50\%}$	3.0	3.3	3.0	1.12	$\mathbf{M}^{90\%}$	2.8	2.7	3.4	1.13
$\mathbf{T}^{50\%}$	3.1	3.0	4.7	1.04	$\mathbf{A}^{50\%}$	2.9	2.7	3.9	1.10
$\mathbf{T}^{60\%}$	2.9	3.4	4.7	1.07	$\mathbf{A}^{60\%}$	3.0	3.7	4.3	1.14
$\mathbf{T}^{70\%}$	3.1	4.4	3.9	1.08	$\mathbf{A}^{70\%}$	3.0	4.2	4.5	1.11
$\mathbf{T}^{80\%}$	2.9	3.5	6.0	1.10	$\mathbf{A}^{80\%}$	2.9	2.7	4.2	1.04
$\mathbf{T}^{90\%}$	2.9	5.2	6.7	1.16	$\mathbf{A}^{90\%}$	2.9	4.2	4.3	1.09

[a]Expected (theoretical) M_n value based on an assumption of linear molar mass growth with monomer conversion, where monomer conversion was monitored using ^{1}H NMR spectroscopy. [b]Measured by ^{1}H NMR spectroscopy using end group analysis based on norbornene end group proton integrations compared to backbone proton integrations. [c]Measured by SEC in THF at 30 °C using light scattering and refractive index detectors using d*n*/d*c* values noted in the Experimental Section.